The impact of climate change on rainfall extremes over Northeast Africa

Bas de Boer

August 6, 2007

Contents

Abstract

Africa is highly vulnerable to rainfall variability and thus to climate change. The highest impact of this variability is through extremes, such as floods and long periods of severe drought. In this study, these extremes in rainfall have been investigated.

For comparison, rainfall extremes over Northeast Africa, which includes Ethiopia and Sudan, have been analyzed in the ERA-40 reanalysis dataset. The analysis showed three clear signals during rainfall extremes. (1) A negative connection with Sea Surface Temperatures (SSTs) in the equatorial Pacific Ocean, i.e. ENSO. (2) A positive connection with the Tropical Easterly Jet (TEJ) at 200 hPa, which overlies the region, and (3) a positive connection with moisture advection over central Africa, southwest of the region.

The second part of the study focuses on the projected changes under global warming of extreme precipitation events in a model ensemble of the ECHAM5/MPI-OM GCM. In the model, the future climate period of 2051-2100 is compared with the present climate between 1951 and 2000. The rain season, from May to October, is projected to shift towards later in the season. In terms of rainfall extremes, for both tails the magnitude is projected to decrease in June and July, and increase from August to October.

The climate signals found in the ERA-40 dataset are analyzed on their changes under global warming, and if they can explain the projected changes in rainfall. The strongest connection is found for the moisture advection southwest of the region, from which changes in the 10% largest extremes coincide quite well with the projected changes of wet extremes. Similar results are found for the TEJ, although the correlation is weaker.

The connection with the dry extremes was less evident and could not completely be address to either the TEJ or to changes in the moisture advection. Furthermore, changes of the ENSO signal where not found in the model, but both the present and the future climate showed a significant and negative correlation between ENSO SSTs and rainfall in the region.

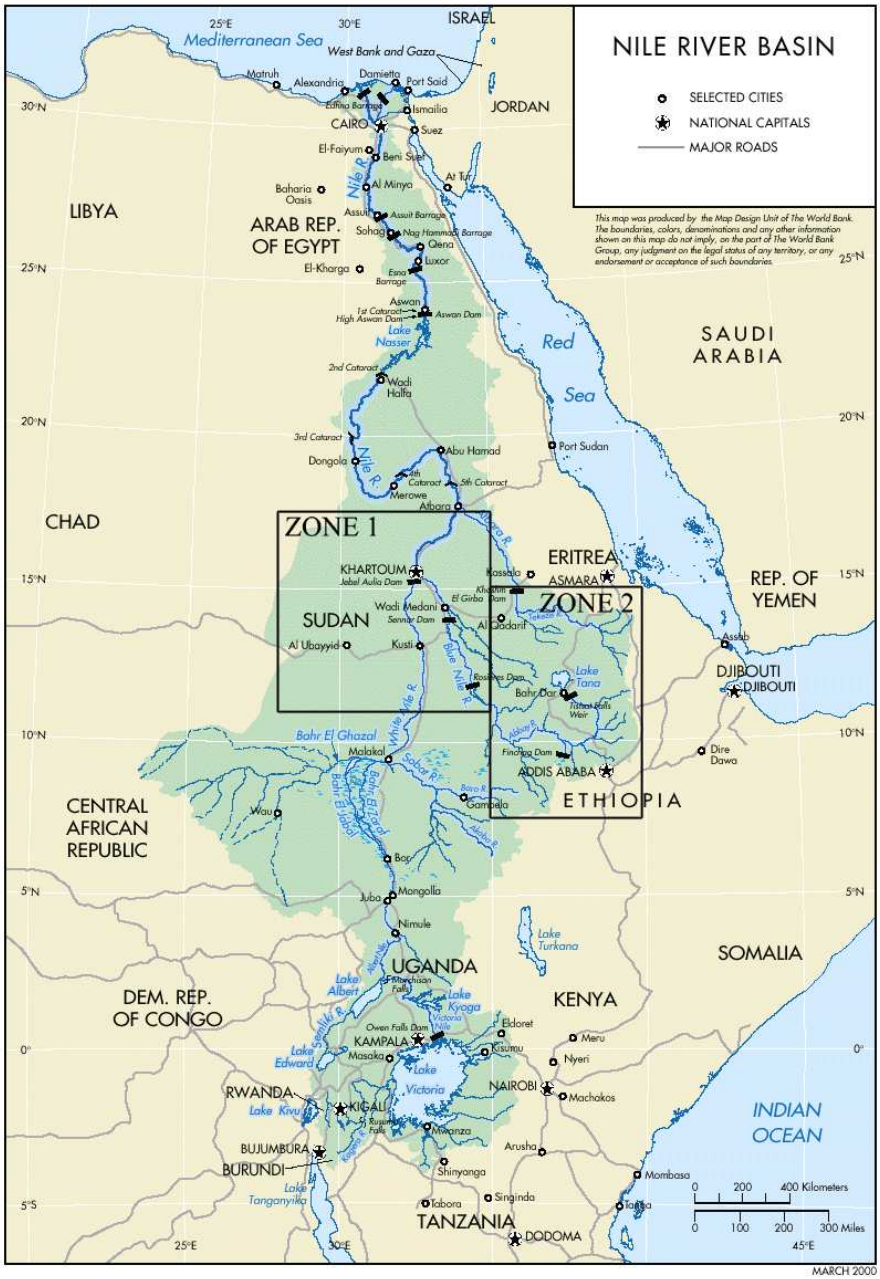

Figure 1: The Nile river basin, with the two analyzed regions, zone 1 over Sudan and zone 2 over the Ethiopian Highlands.

1 Introduction

Climate change is one of the hottest topics (literally, if we talk about global warming) of current literature on climate. The most prominent publication on this topic is by the Intergovernmental Panel on Climate Change (IPCC), which releases a vast and comprehensive overview on climate change every 6 years, with the Fourth Assessment Report (AR4) published this year (IPCC AR4 2007 [9]).

In the AR4 and other "Climate Change" literature (e.g. Hulme et al. 2001 [8]) and Held and Soden 2006 [5]), most attention is focused on the changes in temperature and rainfall, especially on the mean state of these two variables. This research focuses on the projected changes under global warming in extreme precipitation events in Africa, with the main focus on Northeast Africa, which includes Ethiopia and Sudan, as shown in Figure 1.

Extreme events, such as floods and droughts, are of major concern to Africa, since the continent is highly vulnerable to rainfall and temperatures variability and thus to climate change. With respect to the above named two countries, both have a large number of people who are living in the rural (non city) areas. In Ethiopia, this is the case for 80% of its ever increasing population.

The consequences of variability of rainfall on the rural areas, is mostly noticed through its impact on the complete hydrological cycle, e.g. evaporation, water content of the surface and runoff of rivers. Especially the latter is of major concern to the Sudan area, since it is highly dependent on runoff of the Nile, which is fed by the Blue Nile in Northern Ethiopia (about 70%) and the White Nile flowing from Lake Victoria (Conway, 2005 [1]). Also, with the likely increase of the temperature the loss to evaporation is also likely to increase. Since water management and food security are both poor in the region, rainfall variability will have the largest impact on this section of the population, whom are highly dependent on profits from agriculture, which in turn is largely affected by rainfall variability.

The impact not only depends on the amount of rainfall, whether it is a shortage or excess, but also on the duration the event persists. In case of short term changes in rainfall such as a single day (or a few days) the impact is not that severe, and adaptation would not be necessary. But, for example, in case of a long period of drought, the impact on the region is far more stronger, and adaptation is necessary. This is mostly in the hands of governmental institutes who are concerned with the above stated topics, i.e. water management and food security.

This study is part of a more broader research project about projected precipitation extremes in whole Africa, for which results can be found on: Climate Change in Africa (2006 [17]). This has been further extended in the studies of Shongwe et al. (2007 [18]) and Endalew (2007 [2]). Although the methods used are quite different, the core of there research is the same; investigating the impact of climate change on precipitation extremes in Africa.

For this region, and others shown on the website, the monthly mean precipitation of the CRU TS 2.1 dataset has been compared with 23 Global Circulation Model (GCM) simulations which contributed to the IPCC report (AR4 2007 [9]), to select the best models for the region. The comparison consists of two variables, the linear correlation as explained later on, and the RMS error. The former indicates how well the model simulates the rainfall in pattern and timing, while the latter indicates the difference in magnitude between the model and the observations.

In case of correlation a number of GCMs had a very good fit with the observational data, however, the RMS error indicates that there is a difference in magnitude between

the simulations and the CRU observations. As can be seen in Table 1, which show the top 4 models, the ECHAM5/MPI-OM GCM is highly correlated with the CRU observations. Therefore, the ECHAM5 model is used in this study, as a 17 member ensemble run.

Table 1: The May to October averaged correlation and RMS error for the 1951 to 2000 mean climatology over Northeast Africa of the IPCC GCMs.

Model	**Correlation**	**RMS error**
ECHAM5/MPI-OM	0.922	0.864
GFDL CM2.0	0.902	1.343
GFDL CM2.1	0.902	1.277
UKMO Hadgem1	0.918	0.964

This study gives an overview of projected changes of (extreme) precipitation during the rain season in the ECHAM5/MPI-OM Coupled Ocean-Atmosphere GCM over Northeast Africa. In addition, the possible causes of floods and droughts, such as changes in the upper and lower atmospheric circulation and Sea Surface Temperatures (SSTs), have been analyzed. Therefore, the main goal of this research is to answer the following question:

What are the projected extreme precipitation changes (i.e. flooding and drought) over Northeast Africa in the ECHAM5 GCM ensemble, and what could be the cause of these changes?

Previous studies have proposed several causes for rainfall variability, and thus changes in rainfall extremes, over Africa. The most apparent cause is that of changes in SSTs of the oceans. More specific, climate variability is remotely forced by the ocean, and amplified by local land-atmosphere interaction (Giannini et al. 2005 [4]). In this matter, the El Nino/Southern Oscillation (ENSO) phenomenon in the Pacific Ocean has been shown to have an effect on the climate in Africa (a.o. Tippett and Giannini 2006 [20]). Also the Atlantic and Indian Ocean, have shown to be linked to changes in rainfall (Hoerling et al. 2006 [6]).

Section 2, gives an overview of the climate of Africa and in particular Northeast Africa, from observations of the 20th century. Next, the first part of this research, Section 4, will be an analysis of extreme precipitation events with the ECMWF ERA-40 reanalysis dataset, from which the results will be used in the final section, Section 5, to investigate the projected future climate changes in the ECHAM5 ensemble.

2 The climate of Africa

Both the observed temperatures and precipitation are taken from the Climate Research Unit (CRU) TS 2.1 0.5° observational dataset (Mitchell and Jones 2005 [12]), from which the mean climate from 1971 to 2000 has been used as climatology.

The climate of the continent is quite diverse, largely a cause of its position, which is almost completely within tropical latitudes, from 35°S to 37°N. Therefore, the climate is mainly controlled by the Intertropical Convergence Zone (ITCZ) and the subtropical high pressure cells on either side of the equator (S.E. Nicholson 2000 [13]). Also the elevation above sea level has an influence on the local climate. In some areas, such as the Ethiopian highlands, the climate is changed from tropical to a subtropical or even cooler type of climate due to its high orography (from The Climate of the Earth 1985 [10]).

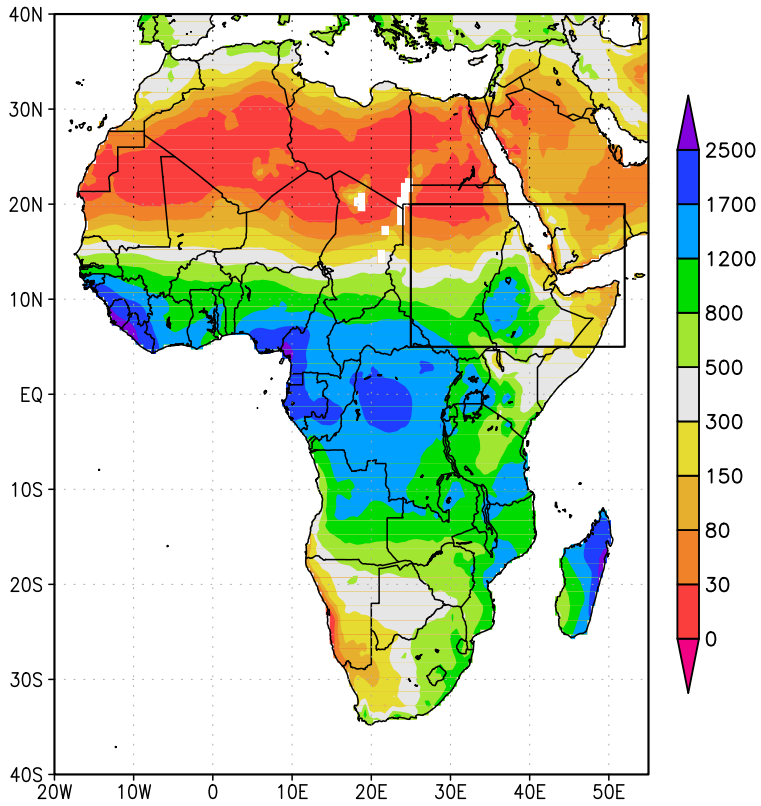

Figure 2: The CRU data 1971 to 2000 mean total annual precipitation (mm) for Africa with the boundary (black box) of Northeast Africa.

As shown in Figure 2, the region of Northeast Africa (indicated by the box) contains a large part of Sudan and Ethiopia and the northern part of Somalia (i.e. the Horn of Africa). Also, the two sub-regions (which will be called zones) are shown in Figure 3. Zone 1 is situated in Sudan and has a semi-arid climate, zone 2 includes the Ethiopian highlands and is much wetter but has lower temperatures. Furthermore this zone includes the Blue Nile which serves as a major source for the total water of the

Nile river. Although both zones have a total different climate, the season of maximum precipitation is the same, from July to September (i.e. the northern hemisphere, or boreal, summer).

2.1 Precipitation and Temperature

The total annual precipitation, as is shown in Figure 2, is quite different over the continent, by far the most precipitation falls in western Africa, on the west coast at the Atlantic Ocean and around the Gulf of Guinea. Also a maximum in precipitation is clearly present in the Ethiopian highlands and on the east coast of Madagascar. Also the peak in rainfall, the length of the rain season and the seasonal character are very different across the continent.

As is shown in Figure 3 the larger part of Northeast Africa is quite dry, especially the northern part (Sahara desert) and the Horn of Africa (Somalia) are very dry areas. The total annual rainfall exceeds well above 1000 mm/year (even near 2000 mm/year has been measured) for the highlands and around 300 mm/year for the Sudan region. The latter region contains the Sahel, which is the transition zone from the wet tropical region to the dry Sahara desert. Therefore, a large north to south gradient is present in Sudan with values below 100 mm/year for the northwestern part of the region.

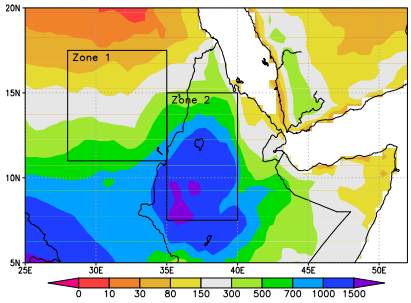

Figure 3: Similar to Figure 2, but for Northeast Africa, with the boundaries (black boxes) of zone 1 and zone 2.

Figure 4 shows the mean precipitation and temperature for each of the two zones, depicted in Figure 3. Clearly the boreal summer (July to September) is the main rainfall season for both zones. The main difference is that there is not only much more precipitation in zone 2, but also outside these three month there is significant precipitation (with the exception of December to February). The ITCZ is the main rain bringer to the region.

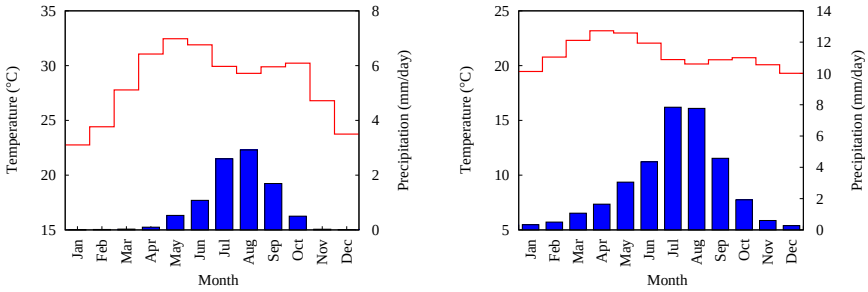

Figure 4: The monthly mean precipitation (mm/day) and temperature (°C) for (a) zone 1 and (b) zone 2. The precipitation is indicates with the blue bars, the temperature with the red line.

Temperature does not vary much in tropical areas, however during the rain season there is a small temperature decrease, when the highest temperatures should be expected (summer on the Northern Hemisphere). This is caused by two mechanism. The first is a reduction of solar radiation reaching the surface, a negative short-wave cloud effect, which is thus higher than the positive long-wave effect of clouds reflecting back the radiation of the earth.

Second, due to an increase in precipitation there is a higher moisture intake of the surface, enhancing the heat capacity of the ground. This means that a given energy flux into the surface will be used preferentially to evaporate the moisture, rather than to heat the surface (Giannini et al. 2005 [4]). Also, the temperatures of zone 1 (a mean of 28.3 °C) are much higher than for zone 2 (a mean of 21 °C), caused by the high elevation of the latter region.

2.2 Circulation

Figure 5 shows the circulation pattern for July/August. The surface position of the ITCZ, which separates the northeastern trade winds and the humid southwestern monsoon flow, lies at about 18° to 20°N. The convergence zone slopes upwards to the south, with the hot dry air from the north flows on top of the tropical humid air from the southwest. Obviously cumulus clouds will form in the tropical air, but due to the temperature inversion that exists at the (sloping) frontal surface, convective activity is limited with height. Therefore, precipitation is located much more to the south than the actual surface position of the convergence zone.

During this season there is another convergence zone present over Africa, called the Zaire Air Boundary (ZAB, the dashed line in the figure). This zone separates the flows off the Atlantic and Indian Oceans, and is a primary rain bringer to the Ethiopian highlands.

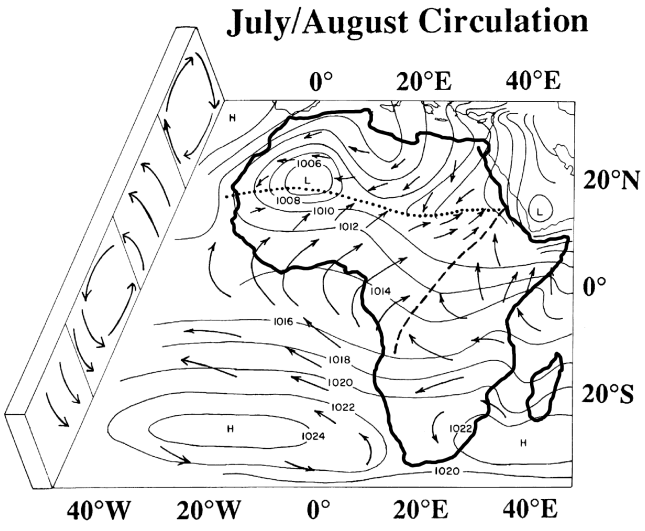

Figure 5: The general patterns of winds, pressure and convergence over Africa for the July and August. Dotted lines indicate the ITCZ, the dashed line the ZAB. (from Nicholson 2000 [13])

2.3 Moisture advection

Moisture advection and divergence of moisture are both important variables with respect to rainfall variability (Held and Soden 2006 [5]). The moisture advection is a combination of two variables, the moisture content of the atmosphere (specific humidity) and the circulation, explained in the previous section. Figure 6a and b show respectively the mean July divergence of the moisture flux (which is highly connected to the difference between precipitation and evaporation, i.e. P-E) and the mean July moisture advection. Both figures are the mean from 1971 to 2000 in ERA-40.

Shown in Figure 6a, the divergence of moisture has quite a distinct pattern, whereas negative values (blue and purple) show sinks of moisture, and are associated with rainfall regions such as the Atlantic ITCZ, central Africa and the Ethiopian highlands (compare with Figure 2). The sources of moisture are indicated with positive values (yellow and red) of divergence, which mainly are the large ocean basins. Naturally, deserts do not serve as a source or sink of moisture, which however does not mean there is no moisture transport over the area, as can be seen in Figure 6b. The moisture transport,

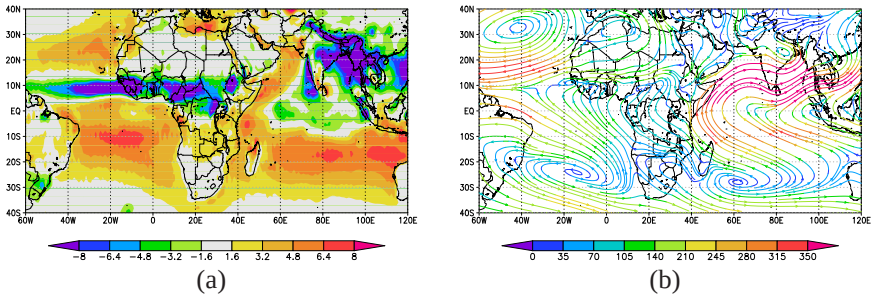

(a) (b)

Figure 6: The ERA-40 mean vertical integrated (a) divergence of the moisture flux (mm/day) and (b) advection of moisture (kg $m^{-1}s^{-1}$) for July.

shown in Figure 6b, is highly linked to the low level circulation pattern, where most moisture is present. The largest moisture transport is located over the Indian Ocean, where large amounts of moisture are transported towards southern Asia, and serve as a major source for the southern Asia monsoon system. But, this large band of moisture transport is also a source for the eastern African monsoon and rainfall in central Africa. The moisture from the Atlantic Ocean is mostly transported into the Atlantic ITCZ and the West African monsoon

To get a more specific view on moisture transport to the region, Figure 7a and b show respectively the total atmospheric column of moisture advection and the advection at the 850 hPa level. The latter clearly shows the large moisture advection from the Indian Ocean, near the coast of Somalia, which is present in the lower levels of the atmosphere and directly linked to the Low Level Jet (LLJ).

The total column of moisture advection is shown in Figure 7a, in which the strong LLJ is clearly visible, together with the inflow from the southwest. This indicates that the largest part of the moisture is transported into the region in the lower levels of the atmosphere, below 600 hPa. Furthermore, the convergence zone of the southwesterlies and northeasterlies is clearly present around 12°N in West Africa and at a more northerly position in Sudan.

In case of zone 1 (central Sudan), most moisture is advected from the southwest and converges with the dry northeasterly flows in northern Sudan, so the Atlantic south-

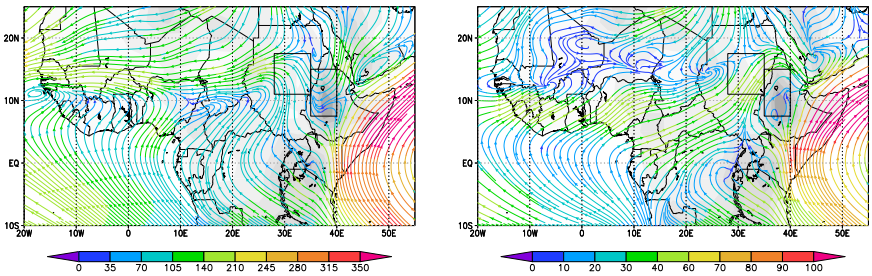

Figure 7: The ERA-40 mean moisture advection (kg $m^{-1}s^{-1}$) of (a) the total column and (b) the 850 hPa level, both for July. The shaded grey indicates the orography.

westerly flow (which also takes up moisture over central Africa, i.e. the Congo) serves as a major source for this region. With respect to zone 2 (the Ethiopian highlands), most moisture does seem to originate from the LLJ, i.e. from the Indian Ocean, although large areas of this region are highly elevated and are well above the 850 hPa level. However, this elevation is not a barrier, but it enhances the rainfall in the region. In case of the other months in the rain season (not shown), the pattern of the moisture advection is quite similar to that in July.

2.4 The Tropical Easterly Jet

Another important climatological feature with influence on rainfall in the region is the Tropical Easterly Jet (TEJ). The TEJ is located in the upper troposphere between 200 hPa and 100 hPa and is positioned around 10°N. The jet exists during the boreal summer months, and is strongest during July and August. As can be seen in Figure 8, which shows the 200 hPa streamlines for July (ERA-40), the TEJ entrance region is over southern Asia and the jet penetrates the African continent up to the western coast.

The TEJ is produced as a result of the thermal induced upper tropospheric anticyclone above the Tibetan plateau. Here, the mid-troposphere is heated directly from the high elevated surface of the plateau, and from latent heat release through orographic induced rainfall. This results into a strong pressure gradient at 200 hPa between the anticyclone over the continent and the low pressure over the summer Indian Ocean, which concentrates into a geostrophic easterly current, which is thus named the TEJ (Hulme and Tosdevin, 1989 [7]).

The relation of the TEJ to rainfall in the region is mostly through its juxtaposition with the ITCZ, for which its highest latitudal position coincides with the maximum strength of the TEJ. The TEJ enhances the uplift in the convergence zone through downward motion on the northern side, and upward motion on the southern side of the jet (Hulme and Tosdevin, 1989 [7]).

2.5 ENSO

The El Nino-Southern Oscillation (ENSO) is a climate phenomenom in the equatorial Pacific and is well known for its influence on climate extremes (in temperature and rainfall) all over the world. ENSO consists of two combined climate variations. The

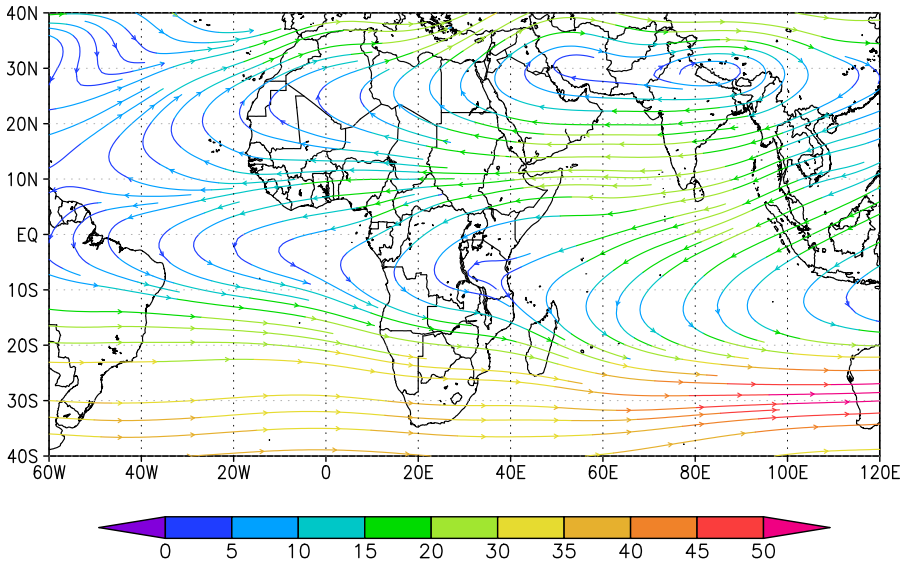

Figure 8: The ERA-40 mean 200 hPa wind speed (m/s) for July.

ocean part is a fluctuation of Sea Surface Temperatures (SSTs) anomalies along the equator and off the west coast of South America. A positive anomaly is called El Nino, while a negative anomaly is called La Nina. The atmospheric part is called the Southern Oscillation (SO) index and indicates the pressure difference between Darwin in Australia and Tahiti in the Pacific Ocean. Also the SO index has positive and negative anomalies for respectively El Nino and La Nina.

The fluctuations in ENSO are reflected in large parts of the world, mainly noticeable as extreme events. For example, during an El Nino, Indonesia and Australia can suffer severe droughts, and heavy rainfall in parts of North America are also likely to occur in the months following an El Nino. Also extreme temperatures, such as a warmer than normal winter in the northern parts of the United States, are known to be an effect of ENSO.

3 Methods

Throughout this study, there are several different analytical, or statistical, methods used to investigate changes in climate, or relationships between different climate indices. This section gives a brief explanation of the used methods, and the two used datasets.

3.1 Correlation

For comparison of two time series, the linear correlation R is a common used statistical value, which states if two quantities are related, i.e. it is a measure of the strength of there relationship. The value of R lies between -1 and 1, with 1 for perfect positive correlation, so the correlated time series increase and decrease together, 0 for no correlation and -1 for perfect negative correlation. In this study it has been used for two objectives, (1) for selecting the models which simulate the observed precipitation pat-

terns best, as explained in Section 1. And (2) for a field correlation of the rainfall time series with other meteorological parameters.

The correlation, or Pearson's r, is given by the following equation:

$$R(x,y) = \frac{\sum_i^n (x_i - \overline{x})(y_i - \overline{y})}{\sqrt{\sum_i^n (x_i - \overline{x})^2 \sum_i^n (y_i - \overline{y})^2}} \tag{1}$$

Here $\overline{x}$ and $\overline{y}$ are the mean values of x and y, and thus $(x_i - \overline{x})$ and $(y_i - \overline{y})$ are the anomalies of x and y. So, for the correlation of anomalies of two different variables, equation (1) is transformed into:

$$R(\Delta P, \Delta var) = \frac{\sum_i^n (\Delta P_i \cdot \Delta var_i)}{\sqrt{\sum_i^n (\Delta P_i)^2 \sum_i^n (\Delta var_i)^2}} \tag{2}$$

Where ΔP_i is a time series of precipitation anomalies and Δvar_i are the anomalies of the correlated variable. Although, there are values of R for all correlations, this does not mean that all relationships are significant. It could well be that the two variables are completely independent and just happen to be correlated, or both are influenced by a third variable not taken into account. To exclude cases like the latter two, the significance of the correlation is measured with the probability (through a student's t-test) of a *zero correlation* (called the Null-Hypothesis, R=0). The probability indicates the chance that the values are not related, from which the significance is determined with a threshold value of the probability, here 5%. The correlation is called significant for 95% if the probability is below the threshold value of 0.05.

3.2 GEV extreme statistics

For the analysis of the extremes in precipitation the Generalized Extreme Value (GEV) distribution is used to fit to the data. With this method, one can calculate return values of precipitation for certain return periods or probabilities. For example, for a return period of 20 years (once every 20 years, i.e. a 5% probability in a year), one can find the return value for the present and for the future climate and thus calculate the changes in extremes.

The GEV distribution is applied to a *sorted* list of maximum values, which are calculated with the block maxima approach. This is done by dividing the data into blocks of equal length (in this case 10 years) and taking the maximum value from each block. For example, from a time frame of 50 years, a list of 5 maxima is obtained. In case of wet extremes the list is sorted from low to high, in case of dry extremes the list of *minimum* values is sorted from high to low.

The list of obtained maxima, or minima, is fitted with the GEV distribution function, which is given by the following equation:

$$F(x) = \exp(-\exp(-x)) \tag{3}$$

where x is called the reduced variate and is given by:

$$x = ln\left[1 + \xi\left(\frac{y-\mu}{\sigma}\right)\right]^{1/\xi} \tag{4}$$

with the constraint that the term between brackets is larger than zero. Furthermore, y is

the fitted data (list of block maxima), $\mu \in \mathbb{R}$ is the location parameter, $\sigma > 0$ is the scale parameter and $\xi \in \mathbb{R}$ is the shape parameter. The return values and times are illustrated with a Gumbel plot, in which the list of block maxima on the y-axis are plotted against the so called Gumbel variate:

$$x = -ln(-ln(F(x))) \tag{5}$$

which is the inverse of equation (3), and equivalent to equation (4), the reduced variate. The function F(x) is defined as: $F(x) = \frac{i}{N+1}$, in which i is the position in the sorted list of maxima and N is the total number of maxima. The fitting equation is obtained by rewriting equation (4) to y as a function of x:

$$y(x) = \mu + \frac{\sigma}{\xi}(\exp(x\xi) - 1) \tag{6}$$

In a Gumbel plot, later on shown in Figure 21, this equation is fitted to the data and can be extrapolated to higher return values and periods. The equivalent return period is calculated with $T = \alpha/(1 - F(x))$ which is adjusted to the Gumbel variate as:

$$x_{per} = -ln(-ln(1 - \frac{1}{\alpha T})) \tag{7}$$

The parameter α is included to correct for the length of the blocks used to calculate the block maxima. Here, a length of 10 years is used and therefore $\alpha = 1/10$. To get a return value for a certain return period, the Gumbel variate of the return period is calculated with equation (7), from which the corresponding return value is obtained through equation (6), in which the parameters, μ, σ and ξ already are known as outcome of fitting this equation to the list of extremes y.

To get an error estimate on the obtained return values, the bootstrap method is used for computing the 95% confidence interval (CI). The method works as followed: the listed data is resampled a number of times (here 1000), according to the *resampling with replacements* principle, for which each list can contain multiple values of 1 data variable of the original list. From each of the 1000 list the three parameters, μ, σ and ξ, are calculated, from which in turn a standard deviation of each parameter can easily be obtained. Next, with the standard deviation for each parameter the CI, and thus an error estimate, for the return values can be calculated.

3.3 Selection of the two zones

The selection of the boundaries of the two zones has mainly been done for all regions as shown on: Climate Change in Africa (2006 [17]), in line of the main project concerning projected changes in extremes in whole Africa.

The zones have been obtained through a so called cluster analysis, as explained in Shongwe et al. (2007 [18], for which monthly observed station data of the Global Historic Climatology Network (GHCN) (Peterson et al. 1997 [15]) have been compared. The cluster analysis looks for similarity in the characteristics of rainfall, i.e. timing and duration, and as a result stations are grouped in clusters, for which the (in this study boxed) area is then defined around the position of the stations. For Northeast Africa two zones could be defined, i.e. zone 1 and 2.

3.4 ERA-40 Reanalysis dataset

The first part of the research has been done with the ERA-40 Re-Analysis dataset (Uppala et al., 2005 [21]) of the ECMWF (European Centre for Medium-Range Weather

Forecasts), in which the data has been obtained from the ECMWF data server. For comparison with SSTs, the NCDC ERSST.v2 dataset has been used (Smith and Reynolds, 2004 [19]). This dataset was constructed from an observational SST dataset, which was also used for the ERA-40 reanalysis. The period considered is similar to the observations, from 1971 to 2000, and from May to October. In case of the extreme analysis, only July, August and September are investigated, since these are the three most extreme months, with the largest anomalies for both zones.

3.5 The ESSENCE project

The second part contains the projected changes in rainfall under climate change, which is done with data of the ESSENCE (Ensemble SimulationS of Extreme weather events under Nonlinear Climate changE) project (ESSENCE project page: [3]). For this project, the ECHAM5/MPI-OM Coupled Ocean-Atmosphere GCM has been used (documentation: ECHAM5: Roeckner et al., 2003 [16], MPI-OM: Marlsand et al., 2003 [11]), to obtain 17 runs with different initial conditions, starting at 1950 and ending at 2100. For the historical period, until 2000, the runs are forced by observed concentrations of greenhouse gases and anthropogenic aerosols. The future climate forcing, from 2000, follows the SRES A1b scenario of the IPCC (AR4 2007 [9]).

The time frame considered is different than that of ERA-40, mainly because of the GEV analysis, for which an as long as possible list of extremes is required. For the present climate (as reference) the analyzed time period runs from 1951 to 2000, while the period of 2051 to 2100 has been used for the future climate. Also here, the analysis has only been done from May to October. An additional reason for this selected period is the possible shift of the rain season, i.e. that it moves out of the three wettest months (i.e. July, August and September). So with broadening the range from May to October, this possible shift will definitely be noticed.

3.6 The IPCC SRES A1b future climate scenario

The following part is literally taken from the Intergovernmental Panel on Climate Change (IPCC) Summary for Policymakers report (AR4 2007 [9]). In the case of the A1b scenario, the total carbon dioxide emission has doubled at the end of the 21st century following a "business as usual" scenario.

The A1 story line and scenario family describe a future world of very rapid economic growth, global population that peaks in mid-century and declines thereafter, and the rapid introduction of new and more efficient technologies. Major underlying themes are convergence among regions, capacity building, and increased cultural and social interactions, with a substantial reduction in regional differences in per capita income. The A1 scenario family develops into three groups that describe alternative directions of technological change in the energy system. The three A1 groups are distinguished by their technological emphasis, in which the A1b scenario is defined as a balance across fossil and non-fossil energy sources. Here balanced is defined as not relying too heavily on one particular energy source, on the assumption that similar improvement rates apply to all energy supply and end-use technologies.

4 Analysis of rainfall extremes in ERA-40

To get a better understanding of the climate in the region, and to know what kind of changes to expect in the GCM simulations, this section contains an analysis of rainfall extremes in the ERA-40 reanalysis dataset. Several fields, which are influenced by, or have influence on rainfall, have been analyzed on their relationship with precipitation in the region.

4.1 Fields during rainfall extremes

To select the extreme months in the dataset the rainfall anomalies where sorted for each of the six months included in the rain season. The anomalies have been computed with respect to the 1971 to 2000 monthly mean climatology from the area averaged time series of the two zones, shown in Figure 3. Especially two years stand out with coinciding wet, or dry, anomalies in more than one month. In case of wet extremes, July, August and September (JAS, i.e. the boreal summer) of 1975 are identified as anomalously wet months, while for the dry months JAS of 1993 has been analyzed. The precipitation anomalies of these two years are shown in Table 2.

Table 2: The selected dates of wet and dry extremes in ERA-40, accompanied by their precipitation anomalies (mm/day). The number between brackets indicates the position in the sorted list of anomalies.

Month	**Year**	**Zone 1 ΔP**	**Zone 2 ΔP**
July	1975	2.357 (5)	2.336 (21)
August	1975	1.661 (8)	5.852 (1)
September	1975	4.167 (1)	5.435 (2)
July	1993	-1.202 (8)	-2.853 (9)
August	1993	-1.702 (2)	-3.863 (2)
September	1993	-1.524 (4)	-3.454 (4)

4.1.1 Precipitation

Shown in Figure 9a and b, are respectively the anomalies for precipitation for JAS 1975 and 1993. Naturally no surprises here, not only there is a rainfall difference within the two zones, also outside the zones rainfall anomalies are similar. Also the temperature anomalies (not shown) are what one should expect. Temperatures are lower (higher) associated with more (less) rainfall in the region, which was previously explained in Section 2.

Next, Figure 10a and b shows the temporal correlation between the area-averaged time series of the precipitation of the two zones with rainfall, as explained in Section 3.1. The result are similar for both zones. Large significant (on the 95% confidence level) positive correlation with rainfall is found in both zones. Small, but significant, negative correlation is found with rainfall around the Gulf of Guinea, similar to the rainfall anomalies shown in Figure 9.

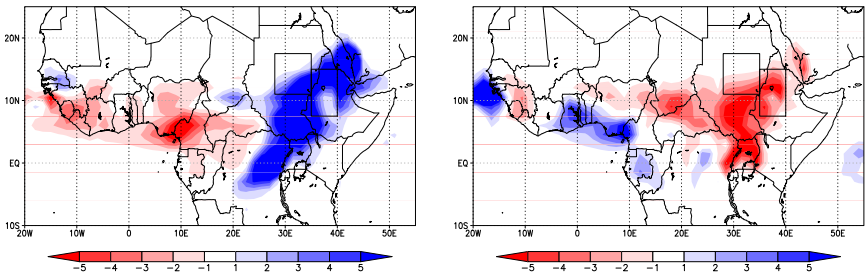

(a) (b)

Figure 9: Anomalies of precipitation (mm/day) for (a) JAS 1975, wet extremes and (b) JAS 1993, dry extremes, difference with the 1971-2000 mean climate. Boxes indicate the areas of zone 1 and zone 2.

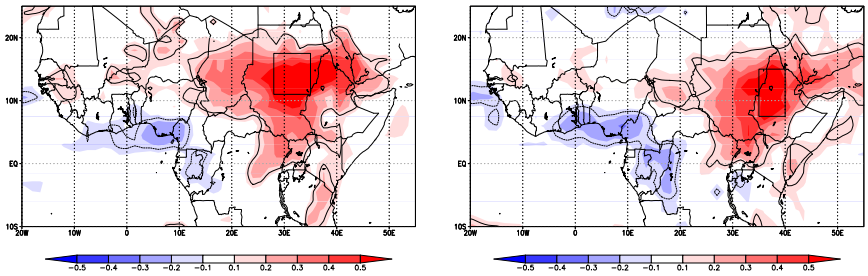

(a) (b)

Figure 10: Correlation R of the rainfall time series of (a) zone 1 and (b) zone 2 with rainfall, for May to October. Solid (dashed) black lines indicate the 95% significant level of R for positive (negative) correlation.

4.1.2 Sea Surface Temperatures

The SST anomalies during wet and dry extremes are respectively shown in Figure 11a and b. Both show clearly an ENSO pattern in the Pacific Ocean, with negative (positive) SST anomalies 2 months in advance of the wet (dry) months. Besides the Pacific Ocean SSTs, the signal in the other large ocean basins are a lot weaker.

Also, correlation of the rainfall time series with ENSO indices (from the NCDC ERSST.v2 dataset; Smith and Reynolds, 2004 [19]), show this negative relation. As can be seen in Figure 12, the ENSO indices, which are area averages of the boxes indicated in Figure 11, have a negative and significant correlation with both rainfall time series for a lag of 2 months, i.e. SST anomalies are 2 months in advance of the rainfall anomalies.

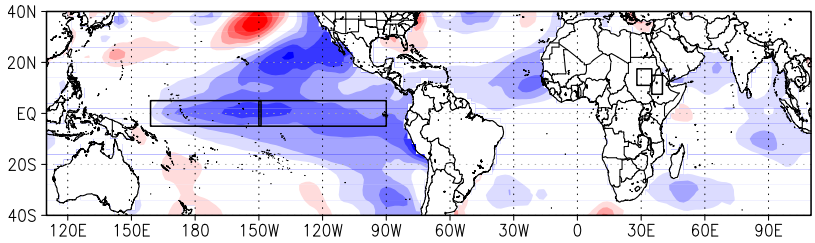

(a)

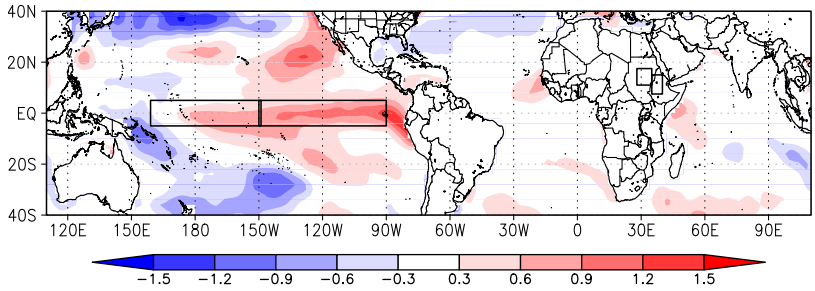

(b)

Figure 11: SST anomalies (°C) for (a) MJJ 1975 and (b) MJJ 1993, 2 months in advance of the rainfall anomalies. The two boxes over the equatorial Pacific indicate the averaging area for the NINO 4 index (left) and the NINO 3 index (right) time series.

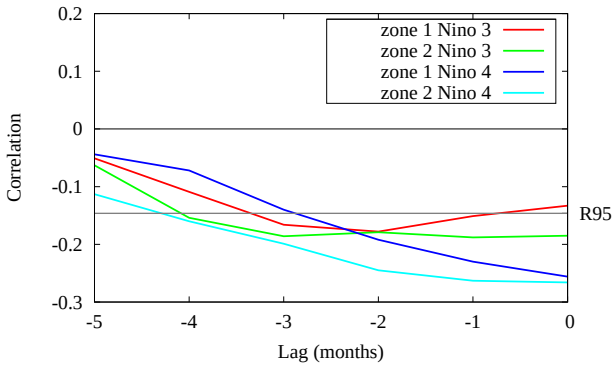

Figure 12: The correlation for May to October precipitation in zone 1 and 2 as function of the lag with two ENSO indices, i.e. the NINO 4 and NINO 3, which are shown in Figure 11. The grey line indicate the 95% confidence level of R, values above this threshold, in absolute sense, are considered significant for 95%.

4.1.3 Upper level winds

Furthermore, also the wind field at 200 hPa (representing the TEJ) shows a strong difference with the climatology during JAS in 1975, as illustrated in Figure 13. The largest anomaly is located over the southern hemisphere, between the equator and 10°S. Since the maximum of the TEJ is located around 10°N, this could indicate a more southerly position of the jet. This is illustrated by Figure 14, which shows the zonal averaged from 25°E to 52°E, west to east velocity at 200 hPa. Clearly the TEJ is stronger for the wet months and is also located more to the south. In case of the dry months (not shown) this signature is much less clear, and does not show a large difference with the mean climate.

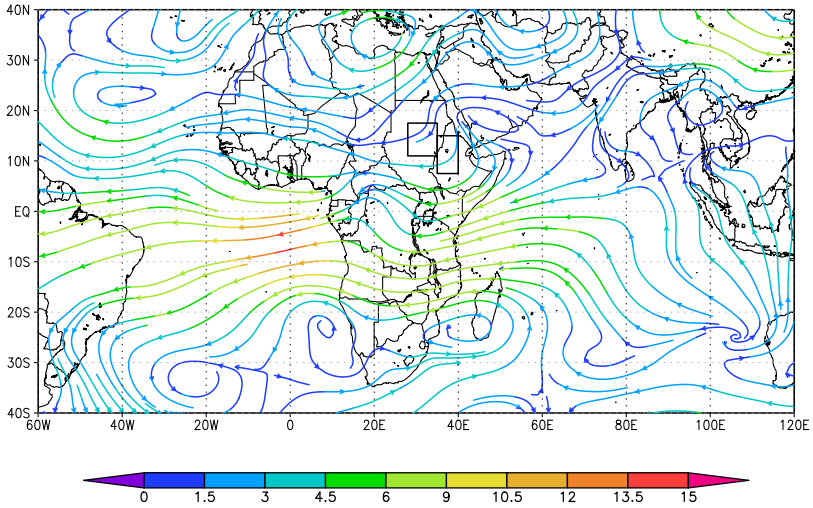

Figure 13: Anomalies of the velocity field at 200 hPa (m/s) for JAS of 1975.

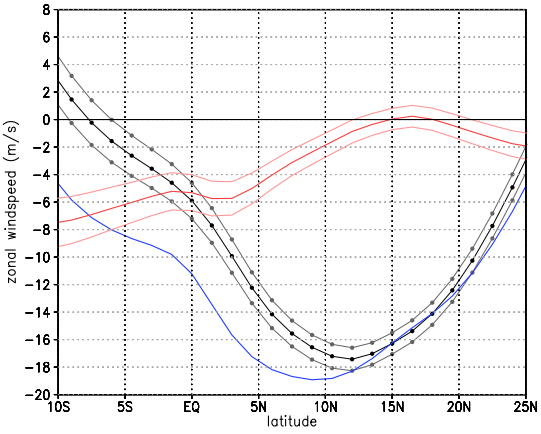

Figure 14: The zonal mean west to east wind speed at 200 hPa (m/s), averaged from 25°E to 52°E. The black line indicated the mean 1971-2000 JAS climate, with grey the 95% CI, the blue line is the JAS 1975 zonal wind during wet extremes, the red line is the difference of JAS 1975 with the mean, with light red the 95% CI.

4.1.4 Moisture advection

As already explained at the beginning of this section, moisture advection is an important parameter with respect to rainfall. Figure 15a and b shows the total column of moisture advection during extreme months, and as can be seen there is an apparent connection between the moisture advection and rainfall extremes. While the mean climatology shows a more prominent supply from the Indian Ocean into the region (Sudan and Ethiopia), the strongest signal for both wet and dry, however, is in the moisture advection from the southwest, indicating a difference in the supply from the Atlantic Ocean. In case of the wet (dry) months the moisture advection from the southwest, over central Africa and indicated by the box in Figure 15, is largely enhanced (reduced), and gives the strongest climate signal of all investigated variables.

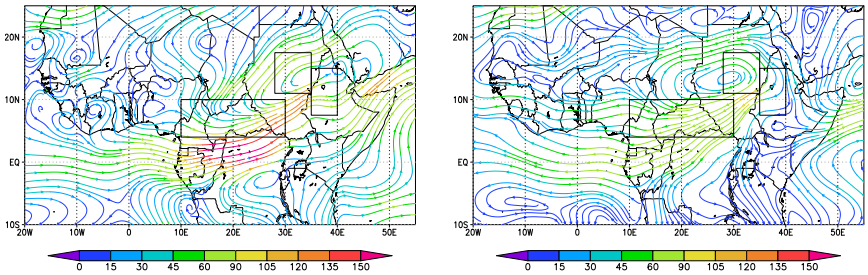

Figure 15: Anomalies of the vertical integrated moisture advection (kg $m^{-1}s^{-1}$) for (a) JAS 1975, wet extremes and (b) JAS 1993, dry extremes. The left box indicates the averaging area used for the time series, also indicated are the locations of zone 1 and 2.

For an even more thorough analysis, the moisture advection has been analyzed during two single months, the wet month of July 1975 and the dry month of August 1993, both shown in Table 2. Both months are a good indication of what is different in the moisture advection during extreme events.

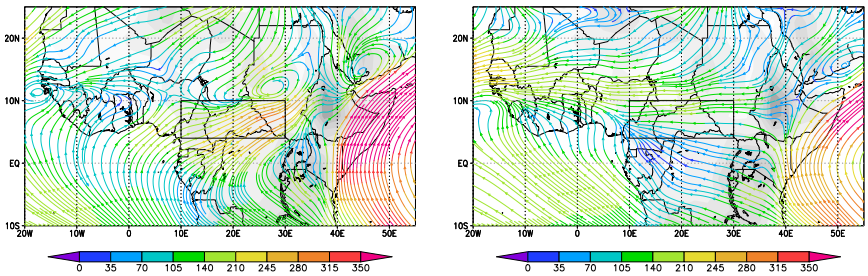

Figure 16: The total vertical integrated moisture advection (kg $m^{-1}s^{-1}$) of (a) July 1975 and (b) August 1993. The box indicates the averaging area used for the hodographs time series.

As can be seen in Figure 16a and b, respectively the moisture advection for July 1975 and August 1993, the patterns are quite similar to the results shown in Figure 15.

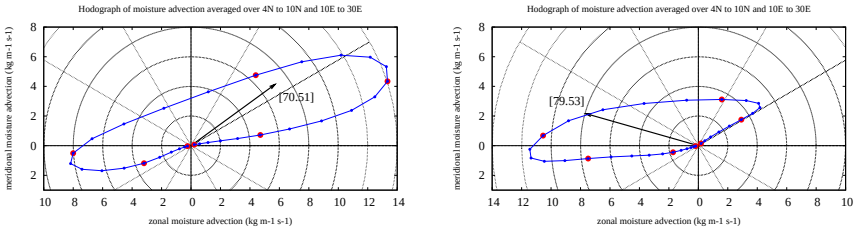

(a) (b)

Figure 17: Hodographs of the moisture advection (kg $m^{-1}s^{-1}$) for (a) July 1975 and (b) August 1993. The red dots are drawn each 5 model levels, starting with level 60 (surface) to level 30 (200 hPa), anticlockwise. The black arrow indicates the direction of the total vertical integrated moisture flux within the area, with its value between brackets.

Within the box southwest of the region, moisture advection is enhanced and directed towards the east for the wet month, while for the dry month the pattern is reversed. The moisture advection as a function of height is illustrated in Figure 17, which is called a hodograph, which shows the area averaged moisture advection of the box indicated in Figure 16.

The moisture advection time series as function of height in the ERA-40 dataset is obtained from 60 model levels, starting from level 60 with the surface pressure to level 1 with a pressure of 0.10 hPa, and an elevation of about 65 km above sea level. The black arrow in Figure 17 indicates the direction of the total column moisture advection (the magnitude is indicated with the number) and can be used to identify the largest contributor to this value, i.e. the level at which most moisture is transported. For both months the maximum in moisture supply is located between model level 55 and 50, i.e. between 1 and 2.5 km height.

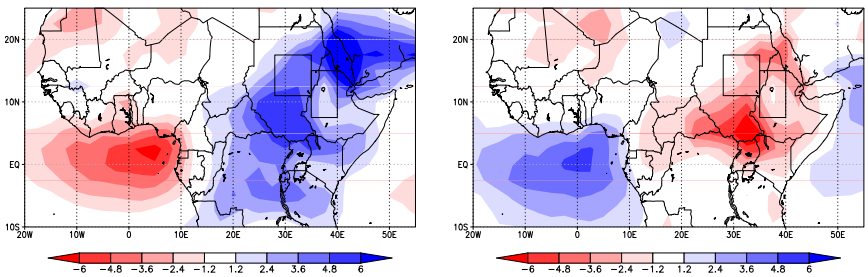

(a) (b)

Figure 18: Anomalies of the total column of water (kg/m^2) for (a) JAS 1975, wet extremes and (b) JAS 1993, dry extremes.

4.1.5 Total column of water

The anomalies of the total column of water (TCW), shown in Figure 18, correspond well with the moisture advection differences during extreme events. In case of a wet event, Figure 18a, the TCW is increased over the region, coinciding with the increase

in rainfall. But furthermore, the TCW is decreased over the Gulf of Guinea. The moisture advection anomaly thus indicates the position of TCW anomalies, i.e. it is directed from the negative to the positive anomaly in TCW. During dry months, the pattern is reversed, as shown in Figure 18b.

4.2 Concluding remarks

As mentioned before, results from the analysis of the ERA-40 dataset will be used later on to investigate the projected changes in the ECHAM5 GCM ensemble. The largest climate signal during extreme events was found in the moisture advection. For both wet and dry months the moisture advection from the southwest shows a distinct difference with the mean climate. In case of a wet month the inflow is increased, while for the dry months the anomaly is reversed. Furthermore, there is a negative connection with rainfall upstream of the positive anomaly. This connection is also found in the total column of water, and through correlation of rainfall with the area averaged rainfall anomalies of both zones.

Clearly the moisture supply from the Gulf of Guinea influences rainfall anomalies in both Northeast and West Africa. In the mean climate the largest part of the moisture, taken up from the southern Atlantic Ocean and over the Congo, is advected towards West Africa. Hence, during wet extremes in Northeast Africa this supply is reduced and serves more as a source for Sudan and Ethiopia. On the other hand, during dry extremes the supply towards West Africa is enhanced. Also it has been shown that the largest amount of moisture is advected in the lower parts of the atmosphere. The anomaly of the moisture advection thus seems to be more an effect of changes in the low level wind than an effect of changes in the moisture uptake of the atmosphere.

Next to the moisture advection also a clear signal during extreme months is found in the upper level winds. Especially during wet extremes the TEJ, located around 10°N, is stronger and has a more southerly position, as shown in Figure 14. In case of dry extremes the difference with the mean climate is very small. Other results, as discussed by Hulme and Tosdevin (1989 [7]), showed a stronger TEJ during wet years and a weaker TEJ during dry years. Furthermore, the results discussed by Hulme and Tosdevin mostly focus on the position of the TEJ relative to the ITCZ, for which the jet is located more to the south (north) during dry (wet) years.

The results presented here are thus in partly agreement with those shown in Hulme and Tosdevin, which also found a stronger jet during wet months. The juxtaposition of the TEJ and the ITCZ has not been investigated here, but the apparent shift to the south as shown in Figure 14 is not in agreement with their results. This difference could be address to the use of a different dataset or observations.

In case of SSTs, the relationship of ENSO with rainfall in the region has been analyzed. As was shown in Figure 11, the field during wet extremes shows a large negative anomalies (a La Nina) over the equatorial Pacific. Although the anomaly during dry extremes is less strong, it is still positive and supported by Figure 12, which shows a negative and significant (on the 95% confidence level) correlation of both zones with two ENSO indices. Significant relationship with the other large ocean basins could not be found. Although there have been studies that linked rainfall variability with SST variations in the Atlantic or Indian Ocean (e.g. Hoerling et al. 2006 [6]), the SST-signal during extreme rainfall in ERA-40 in the latter two oceans was much weaker compared to the ENSO signal.

The dynamics behind this connection is beyond the scope of this research. Nonetheless, other studies have shown possible explanations for the relationship of the ENSO

phenomenon with the African climate. For example, Giannini et al. (2005 [4]) stated that during a warm ENSO (an El Nino) the entire tropical troposphere warms up, and the vertical profile becomes more stable in the tropical region. Hence, deep convection is reduced in the tropical regions, which reduces the amount of rainfall. Also, in the study of Yeshanew and Jury (2007 [23]) it is shown that both the 200 hPa easterly wind and the low level wind from the Atlantic (connected to the moisture advection), are enhanced and related to the Walker circulation, which in turn is influenced by ENSO.

Concluding, Table 3 sums up the found climatological features in ERA-40 during high and low rainfall events in Northeast Africa.

Table 3: Largest climate signals during wet/dry rainfall extremes in Northeast Africa.

Variable	**wet/dry**	**difference with mean climate**
ENSO SSTs	wet	Negative anomalies, La Nina
	dry	Positive anomalies, El Nino
Moist. adv.	wet	Stronger inflow from southwest
	dry	Weaker inflow from southwest
200 hPa wind	wet	Stronger TEJ and winds above the SH
	dry	Somewhat weaker easterlies above SH

5 Climate change as projected with the ECHAM5 ensemble

5.1 Verification of the model

As explained in Section 3.5, the 17 model runs of the ECHAM5/MPI-OM GCM of the ESSENCE project are used for projection of future changes in precipitation in Northeast Africa. Here, the present climate, spanning from 1951 to 2000, is compared with the future climate between 2051 and 2100, which is computed with the SRES A1b scenario of the IPCC (AR4 2007 [9]).

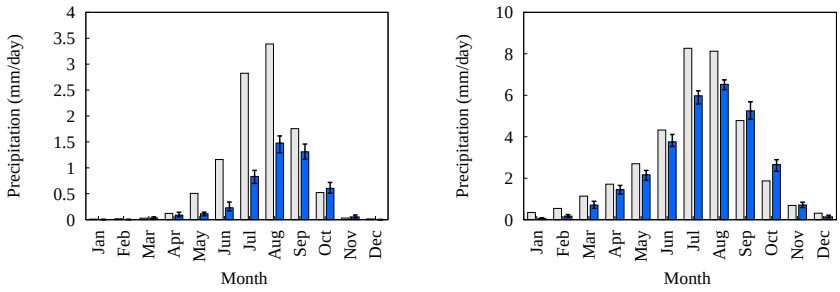

Figure 19: The 1951-2000 monthly mean precipitation of (a) zone 1 and (b) zone 2. ESSENCE rainfall is shown by the blue bars, with the range indicated by the black lines. The observed CRU data is shown by the grey bars.

For comparison with the CRU data, the mean monthly rainfall of the model ensemble and the CRU data are shown in Figure 19, both averaged from 1951 to 2000. As was mentioned before in Section 1, the correlation between the model and the CRU observations is quite high, which, as can be seen, indicates that the pattern of monthly rainfall is simulated well, with high rainfall in July, August and September. However, the model underestimates the rainfall amount of most months, especially for zone 1.

5.2 Projected changes in the mean precipitation

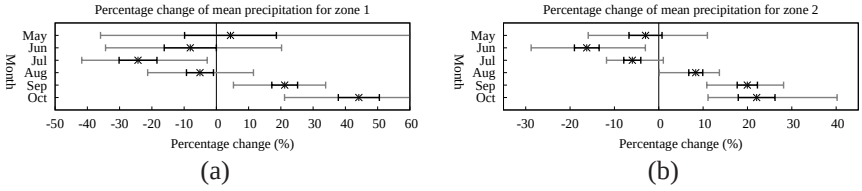

Figure 20: Projected percentage change of the 2051-2100 monthly mean precipitation with respect to 1951-2000, of (a) zone 1 and (b) zone 2. The star indicates the mean value, the black bars the 95% CI and the grey bars the ensemble range, limits outside the boundaries are indicated with the small numbers.

The projected changes of the mean climate in the model are illustrated in Figure 20a and b, respectively for zone 1 and zone 2. The changes are calculated separately for

each realization, and as a result, a *Confidence interval* (CI) is obtained of these 17 runs, which indicates the spread among the members. In other words, if the 95% CI does not include 'zero percentage', one can state (with 95% confidence) that the change is much likely to occur in the ensemble.

For both zones the model projects an apparent shift in the rain season. In case of zone 1, there is a definitive decrease in precipitation in July and an increase in September and October. The CI of both June and August are below zero, but close to no change, i.e. there are a fewer members which show an increase in precipitation. In case of zone 2, the spread is much smaller than for zone 1. Except for May, all months show a CI on one side of the zero percentage line. Therefore, the projected decrease in June and July, and increase in precipitation in August, September and October are significant.

5.3 Projected changes of wet and dry extremes

The projected changes in precipitation extremes for the two zones are calculated with the GEV distribution, as explained in Section 3.2. Two examples of a Gumbel plot are shown in Figure 21a and b, respectively for the 10 year block minima of zone 1 and the 10 year block maxima of zone 2.

As explained in section 3.2, a list of 10 year block maxima, or minima in case of dry extremes, is obtained from each area averaged time series. Since the time span used here ranges 50 years (i.e. a comparison of 1951-2000 with 2051-2100), a list of 5 extreme values is obtained from each ensemble member. The advantage of using a model ensemble like ESSENCE now comes into play. On its own this list of 5 extremes is way too short for making a good fit with this method. But, by combining the whole ensemble of 17 members, the list consist of 85 values (plotted as blocks in Figure 21), which is more than sufficient.

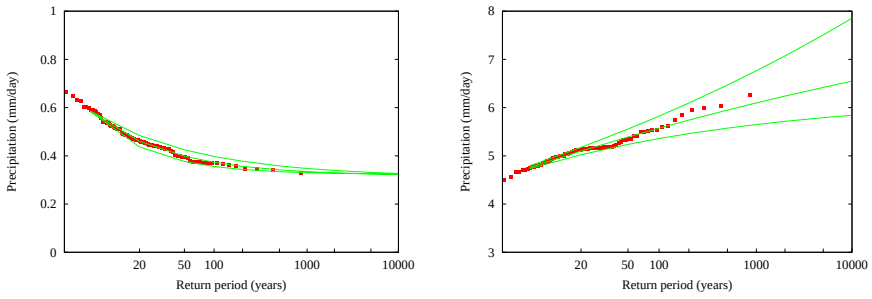

(a) (b)

Figure 21: Gumbel plot of the present climate for (a) 10 year block minima of zone 1 and (b) 10 year block maxima of zone 2. The extreme values (red blocks) are averages from May to October. The green line is the GEV fit as explained in Section 3.2, with the 95% CI.

As can be seen in Figure 21, the return values decrease (increase) with longer return periods for the dry (wet) extremes. The CI interval of the wet extremes becomes wider for larger values, i.e. more uncertainty, while for the dry extremes it stays close to the actual fit, more a cause of the small values, than it is a sign of high confidence.

Similar to the projections for the mean climate, the projected changes in wet and dry extremes return values are also calculated separately for each month, shown in

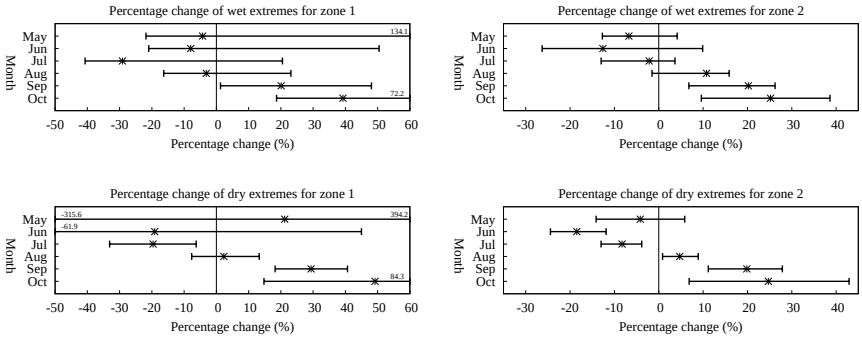

Figure 22: Projected percentage change of the 2051-2100 monthly 1/20 year wet (top) and dry (bottom) rainfall extremes (GEV return values) with respect to 1951-2000, of (a) zone 1 and (b) zone 2. The star indicates the mean value, the black bars the 95% CI (obtained with the bootstrap method), limits outside the boundaries are indicated with the small numbers.

Figure 22. The changes of the extremes look similar to those shown in Figure 20, with higher confidence for zone 2 and months with higher rainfall. For zone 1, Figure 22a, the uncertainty is especially large for May and June, but for both wet (top) and dry (bottom) extremes, the projected rainfall intensity decreases for July, and increases for September and October. In case for zone 2, Figure 22b, the projected changes are more clear, with a decrease in rainfall intensity for June and July, and an increase for August, September and October.

Concluding from these results for the projected rainfall changes, the following list sums up the *expected* climate change projections in the ECHAM5 ensemble of the three climate signals found in the ERA-40 analysis. These expected changes directly follow from their relation with rainfall extremes, as was shown in Table 3.

- For both tails of the rainfall distribution the changes are quite similar, and thus also the expected changes for the moisture advection from the Gulf of Guinea over central Africa should be similar for both the wet and dry extremes. Since the correlation is positive, the moisture advection during extreme rainfall events is likely to decrease in June and July, and increase in August, September and October. The signal during dry extremes could be less evident.

- Although the signal of the TEJ is not that evident, it is likely that the model projects a decrease in strength during high and low rainfall for June and July, and a stronger TEJ during September and October. Furthermore, the easterlies over the Southern Hemisphere are also likely to show similar changes.

- Since SSTs are likely to warm, following global warming, the differences as they occurred in ERA-40, which is lower SSTs during wet events, are difficult to distinguish from the already warmer SSTs. Still, ENSO events should be present in the ECHAM5 ensemble and warm (cold) anomalies are likely to occur about 2 or 3 months in advance of low (high) rainfall events in the region.

5.4 Climate change of other variables

This section contains the projected changes in 2051-2100 with respect to the 1951-2000 mean climate for other fields. With these results, and those later on shown in Section 5.6, the aim is to *verify* the changes listed at the end of the previous section.

5.4.1 Temperature

The largest signal of the projected changes by GCMs is in the global temperature, both SST and land temperature are very likely to increase globally during the 21st century. As is shown by the IPCC (AR4 2007 [9]), the annual temperature increase for East Africa is projected to be between 1.8 and 4.3 °C. This is computed by comparing the last 20 years of the 20th and 21st century, under the same SRES A1b scenario. As can be seen in Figure 23, the temperature increase of the ECHAM5 ensemble is similar to the projected range of the IPCC, but on the high end of this range. With respect to the observations (black boxes), the model captures most temperature extremes in the 20th century. Furthermore, both regions have about the same pattern in the 20th century, with low temperatures during the 1950s and 1960s and an increase in temperature after the mid 1970s.

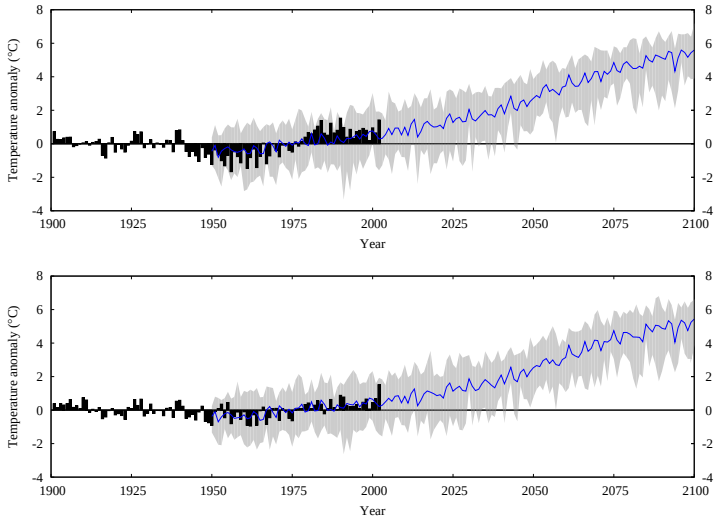

Figure 23: mean May to October temperature anomalies (°C) from the 1951-2000 mean for zone 1 (top) and zone 2 (bottom). Black bars are the CRU observations, the blue line the ECHAM5 ensemble mean and the grey area the range of the 17 GCM runs.

5.4.2 Sea Surface Temperatures

Similar to temperatures above land, also SSTs are likely to increase during the 21st century. The difference between the future and present climatology in the ECHAM5 ensemble are shown in Figure 24, averaged from May to October. Naturally, as can be seen there is no uniform warming over the globe. The most evident differences concerning all oceans is the stronger increase of the Northern Hemisphere and the

stronger increase of the equatorial Pacific area. For each month separately (not shown), the changes look similar, with the strongest differences in the equatorial Pacific area, for which in May and June the increase is stronger than in the other four months.

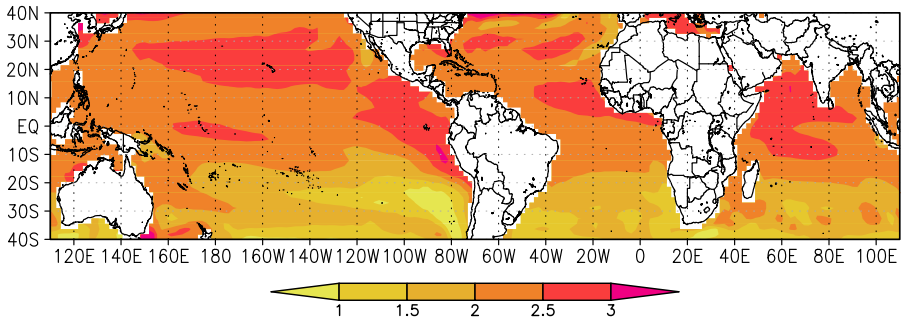

Figure 24: Difference in SSTs (°C) between the future and present climatology, averaged from May to October.

5.4.3 Upper level winds

For most months the mean climate of the TEJ at 200 hPa is projected to show a small decrease in strength. Except for the last two months of the rain season, when the retreat of the TEJ is in full progress, the changes are very small and rather insignificant.

5.4.4 Moisture advection

As was shown in the ERA-40 analysis, an evident signal was found for the moisture advection during wet and dry months. The projected monthly mean changes (not shown) however, do not give such a good indication for changes in precipitation. The region of interest, i.e. central Africa, has very little changes. Only in the first three months of the rain season the mean moisture transported towards the region is projected to decrease. However, the difference between future and present climatology is very small.

5.5 Fields during rainfall extremes

Similar to the analysis of the ERA-40 dataset, the average of extreme events in July, August and September (JAS) have been analyzed for both zones and both tails of the distribution in the ECHAM5 model ensemble. First, the three most extreme events in the whole ensemble of each of these three months (so a total of 9 events) have been selected for both the present and the future climate to verify the fields found in the reanalysis data, as shown in Section 4.1. A further analysis of the changes during rainfall extremes can be found in Section 5.6, followed by the final results and conclusions of the ECHAM5 ensemble analysis.

5.5.1 Precipitation and temperature

The precipitation signal of the selected months is weaker for the dry months, and somewhat weaker for zone 1 with respect to the anomalies in zone 2. The largest precipitation anomalies for JAS are thus found in zone 2. Similar to the results found with

ERA-40, see Section 4.1, temperatures above the surface are lower during the wet months and higher during the dry months. This is both the case for the present and for the future climate. Since temperatures show a strong increase in the ECHAM5 ensemble, as was shown in Figure 23, the anomalies for the future climate where analyzed with respect to the mean climate of the future.

5.5.2 Sea Surface Temperatures

The signal of the SSTs is again strongest in the equatorial Pacific Ocean, i.e. the ENSO region. As shown in Figure 25a and b, respectively the SST anomalies during wet and dry months in zone 2, the signal is clear for the NINO 4 index. However, in the eastern equatorial Pacific the signal is positive, but small, for the wet extremes and thus opposite to the results shown in Section 4.1.

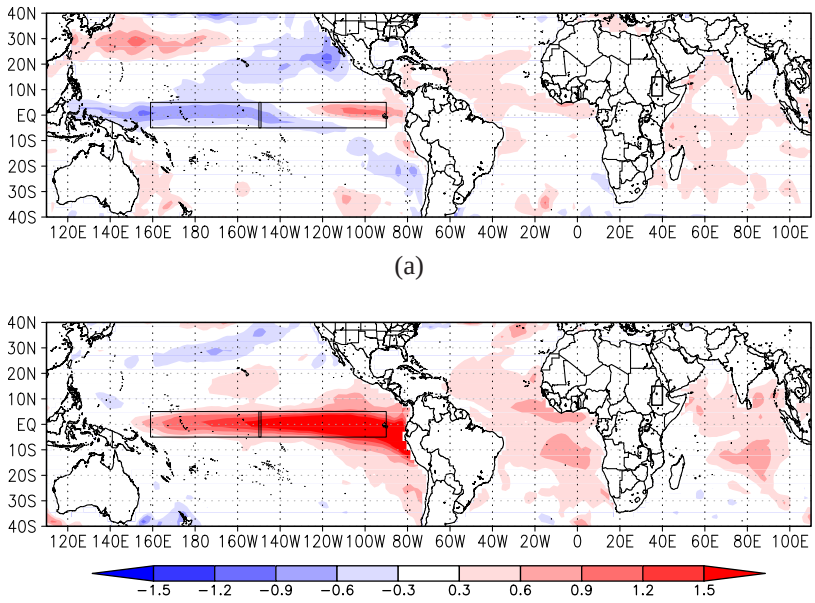

(a)

(b)

Figure 25: Averaged SST anomalies (°C) of 9 wet months in JAS for zone 2 (a) wet and (b) dry extremes in the present climate. Indicated are the boxes of NINO 4 (west Pacific) and NINO 3 (east Pacific), and the box of zone 2 in Northeast Africa.

5.5.3 Upper level winds

The second strong climate signal listed in Table 3 is found in the wind field at 200 hPa. Again the fields look similar the those found in the reanalysis data, with strong anomalies in the TEJ area (around 10°N) and over the Southern Hemisphere. The anomalies are directed westward during the wet months and eastward during dry months. Especially for zone 2 the signal is strong, as shown in Figure 26. For zone 1 the anomaly is much less pronounced and is also much less zonally directed than the anomaly shown in Figure 26.

5.5.4 Moisture advection

One of the strongest signals found in the ERA-40 analysis is a moisture advection anomaly directed towards the region, and located over central Africa, southwest of the region. Also, this anomaly is found in the ECHAM5 ensemble, for both present and future climate and for both zones. The signal is similar to the one found previously, although it has a slightly more northerly position. One example is shown in Figure 27, for the JAS wet months of zone 2 in the present climate. During the dry months, the signal is weaker and opposite to the one shown in Figure 27.

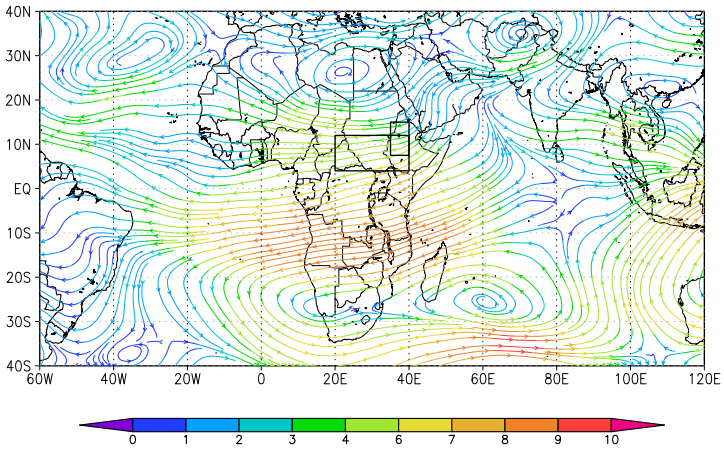

Figure 26: Averaged 200 hPa wind anomalies anomalies (m/s) of 9 wet months in JAS for zone 2 in the present climate. The larger box indicates the boundary of the averaging area for the TEJ time series, with the smaller box indicates the boundary of zone 2.

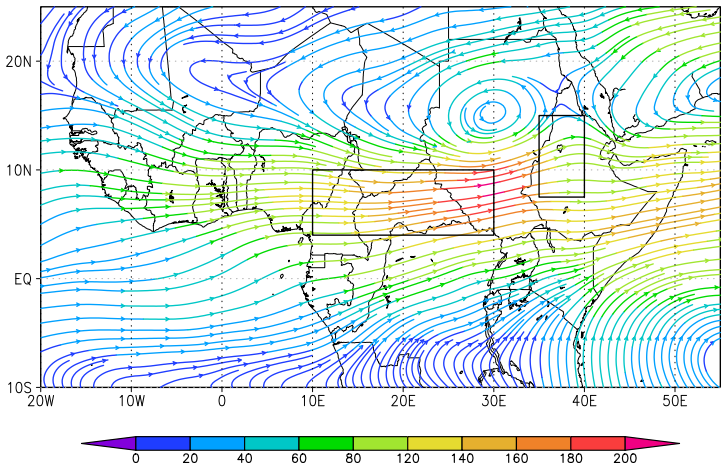

Figure 27: Averaged moisture advection anomalies (kg $m^{-1}s^{-1}$) of 9 wet months in JAS for zone 2 in the present climate. The right box indicates the averaging area for the time series, the left box shows the boundaries of zone 2.

5.6 Projected changes during rainfall extremes

Generally, the fields discussed in the previous section show similar results to the ones found in the reanalysis dataset of ERA-40, so this is a good indication that the model simulates the climate well. But there is still one final question to answer here: what could be the cause of the projected precipitation changes shown in Section 5.3?

5.6.1 Climate change and ENSO

The ENSO climate signal is widely used to predict climate in many parts of the world. For example, its connection with tropical cyclones in the Atlantic is used to make a seasonal forecast for the hurricane season, i.e. what is the expected number of storms and how many will grow into a hurricane. In case of its influence on Northeast Africa, the climate signal could be used as a forecast for severe floods or droughts.

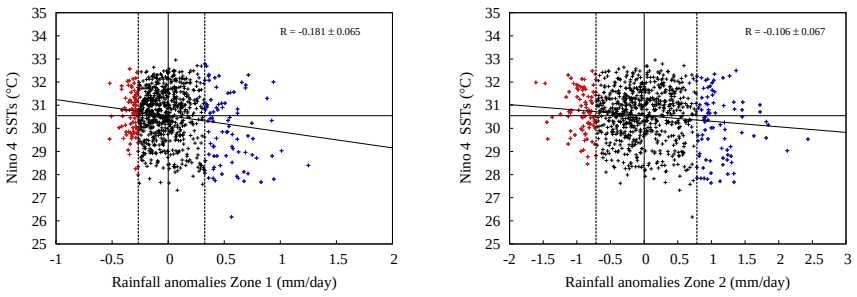

(a) (b)

Figure 28: Averaged rainfall anomalies from May to October (mm/day) for (a) zone 1 and (b) zone 2, plotted against the NINO 4 index SSTs (°C) for the future climate scenario A1b, averaged from March to August. The dashed lines indicate the boundaries for the largest (blue) and lowest (red) 10% precipitation anomalies, the horizontal solid line shows the mean value for the NINO 4 SSTs index.

But what about ENSO in a changing climate, is there a change in the frequency and strength of ENSO? This has been already investigated by Oldenborgh et al. (2005 [14]), in which exactly this question is answered for a large number of GCMs used by the IPCC (AR4 2007 [9]). The climate change influence on the models is investigated with changes in the sea level pressure, representative for the SO index, the atmospheric part of ENSO.

In case of the ECHAM5/MPI-OM model, the change of ENSO is investigated under the SRES A2 scenario. Although different from the here used A1b scenario, the results are labeled as 'highly confident', and thus are assumed to be representable. The ECHAM5/MPI-OM model does show a small shift, but the overall conclusion of Oldenborgh et al. is that the influence of Global Warming on ENSO is very small.

The relationship between ENSO SSTs and rainfall for the future climate in the ECHAM5 ensemble is shown in Figure 28a and b, respectively for zone 1 and zone 2. The figures show the correlation between May to October averaged rainfall with the NINO 4 index, in case of a 2 months lag of the rainfall. For both zones the correlation is significant on a 95% confidence level, thus showing that the negative relationship also holds for the future climate.

5.6.2 Changes of the 200 hPa wind field

The climate signal of the TEJ is especially noticed during wet extremes. Not only for the TEJ the changes are evident, also over the Southern Hemisphere anomalies of the zonal 200 hPa wind are clearly present during high or low rainfall extremes in zone 1 and 2. The link of the upper level winds with rainfall is more obvious for the TEJ, through its connection with the ITCZ, than it is in case of the winds over the southern hemisphere.

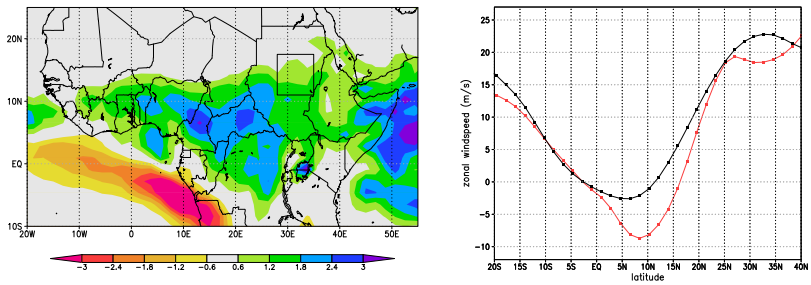

(a) (b)

Figure 29: Projected (a) absolute changes in precipitation (mm/day) and (b) zonal averaged (from 25°E to 52°E) zonal wind at 200 hPa (m/s) during the 20 wettest rainfall events in zone 1 for October. In figure (b), the black (red) line shows the zonal wind for the present (future) climate.

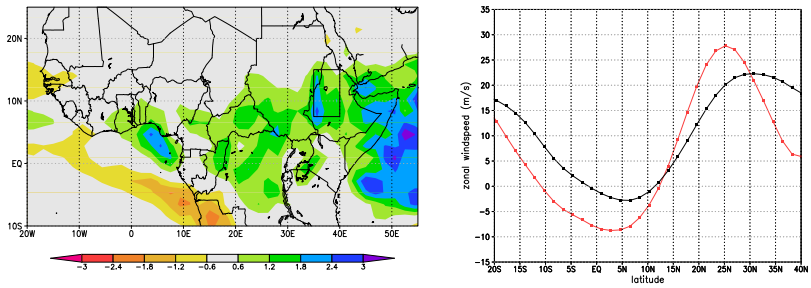

(a) (b)

Figure 30: Projected (a) absolute changes in precipitation (mm/day) and (b) zonal averaged (from 25°E to 52°E) zonal wind at 200 hPa (m/s) during the 20 wettest rainfall events in zone 2 for October. In figure (b), the black (red) line shows the zonal wind for the present (future) climate.

To explain the projected changes in rainfall, shown in Figure 22, the averaged fields of the 20 largest and smallest rainfall events for each month have been analyzed, which are equivalent to approximately a once every 50 years event. For the TEJ, the relationship with rainfall in the region is not in complete agreement for all months. Obviously, rainfall is connected to more variables, and not only depends on the TEJ, for which disagreement does not directly mean that the relationship does not hold at all.

The projected changes of the once every 50 year wet extremes and the coinciding zonal wind field changes in October are shown in Figure 29 and 30, respectively for

zone 1 and 2. In this month, the increased rainfall coincides with a stronger TEJ in October. Actually, the normal conditions in October show an almost complete withdraw of the TEJ, but as is shown in both figures the TEJ is still present, although not as strong as in July or August. Also, the changes above the SH are similar to those in the TEJ region, but for this region the correlation was not significant. Therefore this region was not analyzed any further. Correlation of the TEJ with rainfall was similar to that found for ENSO, as was shown in Figure 28.

5.6.3 The TEJ as a proxy for rainfall extremes

To further analyze the relationship between the TEJ and rainfall extremes in zone 1 and 2 in the ECHAM5 ensemble, anomalies of the upper level winds have been investigated analogous to the extremes in rainfall, to answer the following question:

Can the projected changes in rainfall extremes between future and present climate, in zone 1 and 2, be addressed to changes in the TEJ extremes?

Time series of the TEJ have been obtained from the area average of the box indicated in Figure 26, which partly overlies zone 1 and 2. The extremes of the TEJ have been selected on the 10% (1/10 years) largest or smallest 200 hPa zonal wind anomalies (85 dates), for which the most negative values represents the maxima, and the less negative, or even positive, values represent the minimum values of the TEJ.

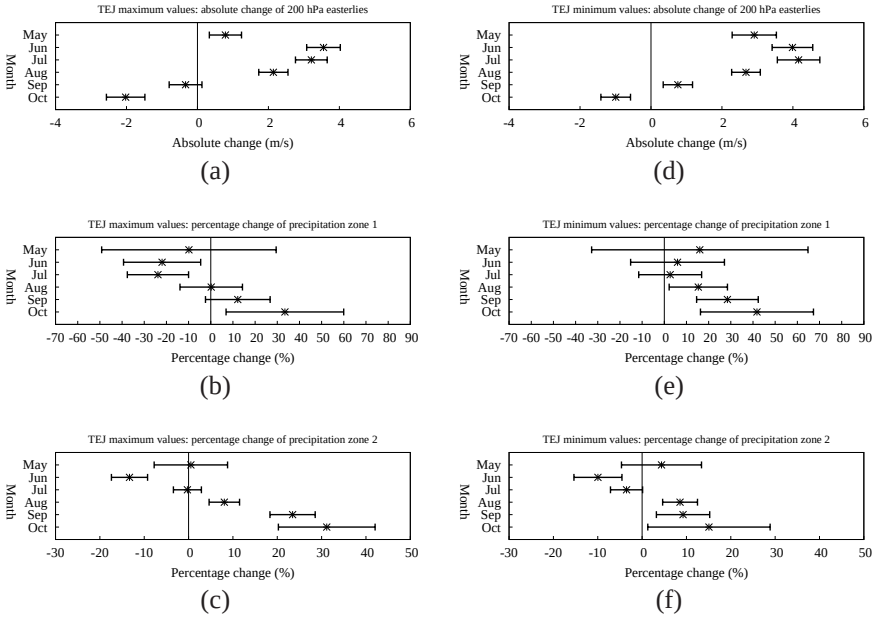

Figure 31: Projected changes of (a) absolute zonal 200 hPa wind, and percentage change of (b) precipitation zone 1 and (c) precipitation zone 2 during the maxima of the easterly 200 hPa wind anomalies over Sudan (4°N to 12°N and 20°E to 40°E). Similar for figures d-f, but for the minimum values of the easterly 200 hPa wind anomalies. The star indicates the mean value, the bars the 95% CI.

The absolute changes of the 1/10 years easterly winds maxima are shown in Figure 31a, which show some similarity with the corresponding rainfall changes shown in Figure 31b and c. Although the changes of the TEJ wind speed are quite small, the increase in TEJ strength in September and October coincides with increased rainfall in both zone 1 and 2. Furthermore, the transition from decreasing to increasing easterlies is somewhat different from the changes in rainfall.

Although small, the changes of the 1/10 year easterly winds minima look similar to the changes for the maxima, as can be seen in Figure 31d. With respect to the rainfall changes, for zone 2 the changes look quite similar, shown in Figure 31f, but for zone 1, shown in Figure 31e, the percentage change of the rainfall is mostly positive for all months. Clearly the influence on rainfall in zone 1 is must less pronounced than for zone 2, similar to the results shown in Section 5.5.3.

5.6.4 Changes in moisture advection

Similar to the TEJ, the same analysis has been done for the moisture advection. Again the 20 most wet or dry rainfall extremes have been selected for each month, as explained in Section 5.6.2. Figure 32 shows the average of the 20 most extreme rainfall events in September, clearly the increase in rainfall is present, which is accompanied by a strong increase in moisture advection from the southwest.

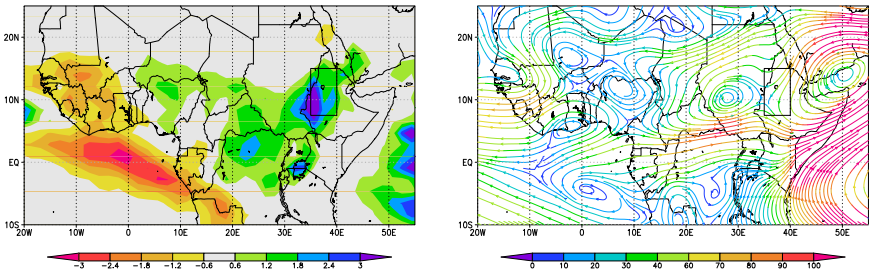

(a) (b)

Figure 32: Projected absolute changes in (a) precipitation (mm/day) and (b) moisture advection (kg $m^{-1}s^{-1}$) during the 20 wettest rainfall events in zone 2 for September.

In most other wet months for zone 2, the correlation between rainfall extremes and moisture advection is present and thus supports the changes in rainfall. For the dry months of zone 1 and 2 the changes are much less significant, with some months show the same relationship and others have a much less clear or different pattern.

The correlation between moisture advection and rainfall for the future climate is shown in Figure 33a and b, respectively for zone 1 and 2. Concentrating on the extremes, shown in red and blue, almost all extreme values of the moisture advection are connected to extreme values of rainfall, which furthermore supports the influence of moisture advection on rainfall.

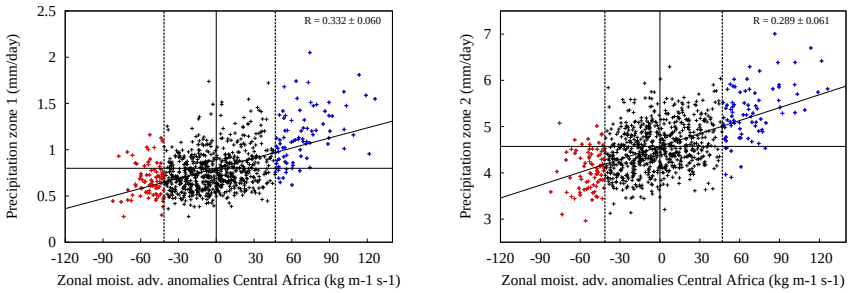

Figure 33: Moisture advection anomalies (kg $m^{-1}s^{-1}$) southwest of the region, plotted against rainfall (mm/day) in (a) zone 1 and (b) zone 2 for the future climate scenario A1b, both averaged from May to October. The dashed lines indicate the boundaries for the largest (blue) and lowest (red) 10% precipitation anomalies, the horizontal solid line shows the mean value for the rainfall.

5.6.5 Moisture advection as a proxy for rainfall extremes

Also, similar to the analysis of the TEJ shown in Section 5.6.3, moisture advection extremes have been analyzed on their influence on rainfall in zone 1 and 2. Certainly, the moisture advection is one of the key parameters which influences the rainfall in the region, and thus the same question is asked:

Can the projected changes in rainfall extremes between future and present climate, in zone 1 and 2, be addressed to changes in the moisture advection extremes southwest of the region?

The time series for the moisture advection have been obtained through area averaging over the box indicated in Figure 27, similar to the box used for ERA-40, as was shown in Figure 16. Since the moisture advection anomaly during extremes shows the biggest change in its zonal component, the extremes have been selected on the 10% (1/10 years) largest or smallest zonal moisture advection anomalies (again 85 dates), respectively called the upper or lower tail. The actual values of the zonal moisture advection are on average negative, so the lower tail consists of large negative values (directed towards the west), while the upper tail consists of small negative, or positive values (the latter directed towards the east).

The absolute changes of the 1/10 year upper tail of zonal moisture advection are shown in Figure 34a. The CI of all months is rather small, indicating that the spread of the 85 maximum values is small. Coinciding with the changes in the zonal moisture advection are the percentage changes in rainfall, shown in Figure 34a and b, respectively for zone 1 and 2. Rainfall changes are calculated with the actual values, not anomalies, but for both the present and the future climate the mean anomalies of both zones are definitely positive, and thus indicating wet extremes.

The changes in rainfall during the upper tail moisture advection anomalies, shown in Figure 34a and b, look similar to the changes of rainfall extremes shown in Figure 22a, and thus supporting the fact that positive moisture advection anomalies in the area southwest of the region do have an effect on positive rainfall anomalies in both zone 1 and zone 2.

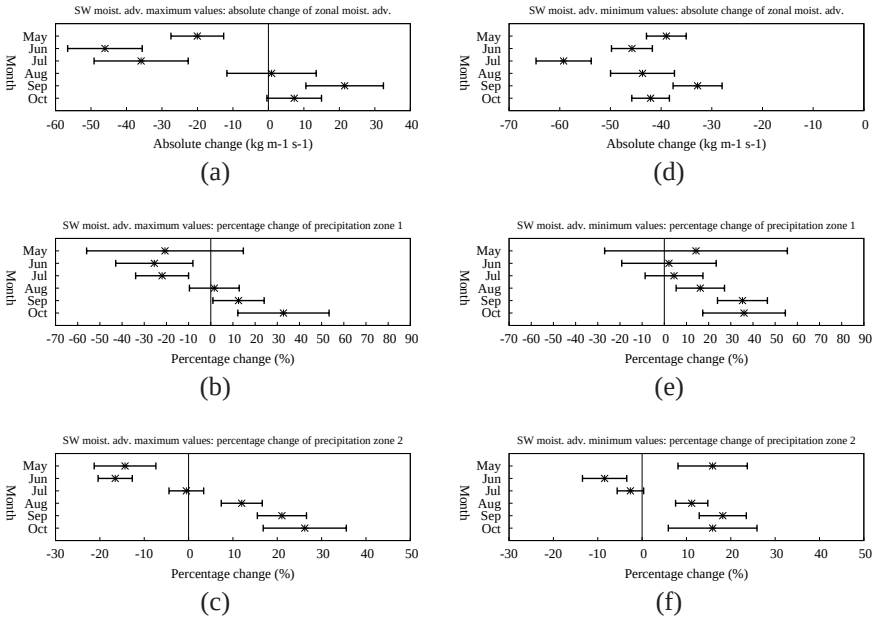

Figure 34: Projected changes of (a) absolute zonal moisture advection, and percentage change of (b) precipitation zone 1 and (c) precipitation zone 2 of the upper tail of the zonal moisture advection anomalies over central Africa (4°N to 10°N and 10°E to 30°E). Similar for figures d-f, but for the lower tail of the zonal moisture advection anomalies. The star indicates the mean value, the bars the 95% CI.

Unlike the percentage change of the upper tail, the lower tail of the moisture advection shows a decrease for all months, as shown in Figure 34d. This is equivalent to an increase in easterly moisture advection directed away from the region. By assuming that the known (positive) connection holds, the rainfall changes should also be negative.

But, as is shown in Figure 34e and f, the changes in rainfall during the lower tail moisture advection anomalies do not match the changes in the moisture advection minima. Although they do show quite some similarity with the changes in rainfall extremes shown in Figure 22b.

6 Summary and conclusions

Northeast Africa is highly vulnerable to rainfall variability, and thus to climate change. Naturally, variability in rainfall is not strange to the whole continent of Africa. In the twentieth century the continent experienced quite some extremes, with both long periods of above normal rainfall and periods of severe drought.

In this study, these extremes in rainfall have been investigated. First, the last 30 years of the twentieth century with the ERA-40 dataset have been analyzed. In order to identify climate signal during rainfall extremes in Northeast Africa. Second, the impact of climate change on rainfall extremes has been investigated with a GCM ensemble.

The main results of this study are the projected changes of rainfall extremes in the ESSENCE ensemble, a 17 member ensemble run of the ECHAM5/MPI-OM GCM with the SRES A1b scenario. The future climate changes are calculated for the period 2051 to 2100, with respect to the present climatology of 1951 to 2000. The projected changes in the mean precipitation, in both zone 1 (Sudan) and 2 (Ethiopian highlands), show a shift in the rain season. For both zones, the mean precipitation is projected to decrease in June and July, while for September and October the precipitation is projected to increase. Furthermore, for zone 2 the shift is 'larger' with respect to zone 1, for which also August is projected to increase, while for zone 1 there is a small decrease in this month.

The changes for the extremes have been calculated with the GEV distribution theorem, for which the once every 20 years return values are used for changes in extremes. For both zones the projected changes of extreme values are similar to the projected changes of the mean precipitation. In June and July both wet and dry extremes are projected to decrease in magnitude, while for September and October the model projects an increase in rainfall intensity. The probability of wet extremes is equivalent to these projected changes. In case of dry extremes this is reversed, so an increase in probability for June and July, and a decrease for September and October for both zones, and in August for zone 2.

As was shown in Section 4.2, the analysis with the ERA-40 reanalysis dataset showed three clear climate signals during rainfall extremes in both zone 1 and 2, which are summed up in Table 3. First of all, a clear signal was found in the SST field during wet and dry extremes, profoundly in the equatorial Pacific Ocean, i.e. the ENSO region. The ENSO climate signal, in general, is known to have a large impact on the climate all over the globe. Although the teleconnection with Northeast Africa is not that well known, fairly large negative SST anomalies where found two months in advance of wet months in both zone 1 and 2 in ERA-40. This connection was found for the JAS rain season and was furthermore supported by the correlation of rainfall time series with ENSO indices, for which all relations showed a significant (on a 95% confidence level) negative correlation.

After the link between ENSO and rainfall variability was established with results from the ERA-40 analysis, the connection was then investigated in the ECHAM5 ensemble. In the model, the relationship is also negative, but now the positive SST anomalies (an El Nino) show the strongest signal during dry extremes in both zone 1 and 2. The signal was strongest for zone 2, which also showed the strongest differences in rainfall. Again the correlation was found to be negative and significant, for both the present and the future climate, but only for the NINO4 index in the western Pacific Ocean.

Although the impact of climate change on ENSO was not investigated, Oldenborgh et al. (2005 [14]) showed that the influence of Global Warming on ENSO is very small,

and thus the ENSO could not be used to explain the projected shift in the rain season in Northeast Africa. Still, the connection in the future climate of the ECHAM5 ensemble was found to be significant. This does not mean that all large rainfall anomalies, negative or positive, are directly linked to large SST anomalies in the (western) equatorial Pacific Ocean. But, it does show that the model projects a continuation of the teleconnection between ENSO and rainfall variability in the region. Therefore, ENSO could be used as a predictor for rainfall extremes in the region.

The TEJ is know to have an influence on rainfall via its connection with the ITCZ (Hulme and Tosdevin 1989 [7]). Although large changes could not be found for the latter, the TEJ did show a strong signal in the ERA-40 analysis, for which it is positively correlated with rainfall in both zone 1 and 2. The signal was especially strong for zone 2, and even more pronounced in the ECHAM5 ensemble analysis. The mean change of the TEJ strength is not that pronounced, but shows a slight decrease in strength during its peak months, July and August. However, the connection between the TEJ and rainfall does not show a strong change, and is quite similar for both the future and present climate.

To investigate the influence of the TEJ on rainfall extremes, extreme values of the TEJ (zonal 200 hPa wind) are used as a proxy, analogue to the method used for the rainfall extremes. So instead of the changes of rainfall extremes, changes of TEJ extremes are analyzed, with their accompanied changes in rainfall. For both tails of the distribution, the largest and smallest 10%, the TEJ shows an absolute decrease in strength from May to August, whereas the maxima show a slight increase in September and both tails show an increase in October. Relatively, the changes are not that pronounced, but show quite some similarity with the accompanied rainfall changes, especially for zone 2.

These changes in rainfall do concern mostly positive (negative) anomalies during the upper (lower) tail of the TEJ distribution, and thus shows that TEJ has a positive connection with rainfall in the two zones. The projected changes of the rainfall extremes, however, could not completely be explained by changes in TEJ extremes, but it is shown that there is a connection between the projected changes in the two variables.

The third and most pronounced signal found during rainfall extremes is that in the vertical integrated moisture advection, for which a strong signal was found southwest of the region, over central Africa. During wet extremes in the ERA-40 dataset, a much stronger inflow of moisture from the southwest was found, whereas during dry extremes the moisture advection is more directed towards the west. Furthermore, this anomaly was shown to be most prominent between 1 and 2.5 km above the surface, i.e. at pressure levels between 850 and 700 hPa.

The moisture advection anomaly not only influences rainfall in the two zones, also rainfall in the Gulf of Guinea, upstream of the positive anomaly, seems to be connected. As was shown in Figure 10 there is a negative correlation between rainfall in both zone 1 and 2 and rainfall in the countries situated along the Gulf of Guinea. This reduction is thought to be an effect of the lower moisture supply to the latter region, since the moisture is advected more towards the northeast. Furthermore anomalies of the total column of water showed the same relation, a positive (negative) anomaly downstream (upstream) of the moisture advection anomaly.

Also in the ECHAM5 ensemble the moisture advection was shown to be the largest signal during rainfall extremes in both zones, whereas the signal was more pronounced during wet extremes. The correlation was largest for this climate signal, and much better correlated with the rainfall than both the TEJ and ENSO time series. Furthermore, the correlation between the moisture advection time series (averaged from 4°N to 10°N and 10°E to 30°E) and rainfall (not shown) illustrates the positive connection

with rainfall in zone 1 and 2, and the negative connection with rainfall along the Gulf of Guinea.

Similar to the TEJ, also changes in the 10% largest and smallest zonal moisture advection are analyzed whether they match the changes in rainfall extremes. As was shown in Figure 34a-c, changes in precipitation for both zones strongly match the projected changes in the 10% most westerly zonal moisture advection anomalies. In the case of the 10% smallest moisture advection anomalies the changes do not match at all, whereas the 10% lowest moisture advection extremes are projected to decrease for all months.

Naturally, rainfall variability does not solely depend on just one variable. In case of wet extremes in both zones the projected changes can be addressed to both the moisture advection and the TEJ. The most westerly extremes of the moisture advection, shown in Figure 34a, show strong similarity to the projected changes of wet extremes, shown in Figure 22. Also, the changes of the TEJ maxima, illustrated in Figure 31a, show quite some similarity. Although these changes are relatively small, the projected increase in October could well be a source for extreme rainfall in both zones.

The projected changes in dry extremes, however, could not be completely explained by changes in the TEJ or moisture advection extremes. In case of the moisture advection this is not so surprising, since the most westerly extremes are already directed away from the region, and thus variability of the moisture advection is largely unnoticed in the two zones. Therefore, changes of these moisture advection extremes, shown in Figure 34d, have little impact on both zones, and thus do not show any connection with the coinciding rainfall changes, shown in Figure 34e and f, or the projected changes of rainfall extremes, shown in Figure 22a.

It should be noted that the method to calculate the extreme values of the TEJ and the moisture advection is different from the GEV theorem used to compute the rainfall extremes. The latter are theoretically computed return values, equivalent to a once in every 20 years probability. The extreme values of the TEJ and the moisture advection are averages of the largest or smallest 10% of all values, equivalent to a once in every 10 years probability. Nonetheless, both are extremes values and representable for changes in extreme events.

Still, there are a lot of unanswered questions, such as the exact cause of the change in the moisture advection. Is it caused by a change in the wind field, or is their more moisture uptake over central Africa? Furthermore, what is the contribution of the Atlantic Ocean/central Africa moisture flow and the Indian Ocean/LLJ moisture flow to the two zones? In other words, can the sources of moisture for the rainfall in the two zones be traced back and quantified?

Furthermore, what was also stated in Section 4.2 and what is shown in a recent study of Yeshanew and Jury (2007 [23]), their could be a connection between the increased moisture advection from the southwest and the increase in 200 hPa easterlies over the Southern Hemisphere. The latter has not been investigated thoroughly, since correlation with rainfall time series where not significant. But, as is suggested by Yeshanew and Jury, this anomaly and the lower level enhanced westerlies are linked to the zonal Walker circulation, which in turn interacts with SSTs in the Atlantic, and is linked to ENSO in the Pacific Ocean. Also, Williams and Nottage (2006 [22]) showed that on a historical point of view high rainfall events in Sudan and Ethiopia are related to a La Nina, a stronger TEJ and a more northerly position of the ITCZ. Therefore allowing more moisture to be advected from the Atlantic, all in agreement with findings of this study.

The main shortcoming in this study is that only one climate model is used in pro-

jecting the changes in rainfall for the region. Although it is a 'state of the art' GCM, and that the model simulates the rainfall pattern quite well for the region, a wider range of GCMs will give a better perspective on the projected changes for the future climate. There are a number of studies whom did include more GCMs (e.g. Hulme et al. 2001 [8] and Shongwe et al. 2007, [18]), for which the projections for this region show a non uniform image for the future climate, and a large range between results of different GCMS. Similar to the finding of the IPCC, (AR4 2007 [9]), the different model projections for rainfall diverge in Northeast Africa, especially for the wet season (as shown in Table 11.1 in Chapter 11 of the AR4).

Nonetheless, climate change will have its impact on the region, whether it will be a more dry season or a more wet season, the climate will always show some variability. However, large deviations from the mean will naturally have the largest impact on the rural areas of the region, for which in case of Ethiopia 80% of its population is part of this group. This large number of people are highly dependent on agriculture for their survival, which in turn is highly dependent on rainfall, i.e. severe drought leads to no growth at all, while flooding lead to the inability to harvest the crops, or even to reach the farmlands.

Therefore, it is important for this region to know the changes in rainfall, not only on this longer climatological scale but also short term weather predictions are very useful in order to adapt to expected rainfall changes.

Acknowledgments

First of all, I would like to thank my supervisor Bart van den Hurk, for giving me the opportunity for doing this study and supporting me when needed. The discussion we had where very useful, and he always gave me an impulse in the right direction. Also, I would like to thank Geert Jan van Oldenborgh for providing the knowledge on programming and climate research and the support in the first couple of months of my stay. Furthermore, thanks to Mxolisi Shongwe, for learning me about the African climate and also answering numerous of question.

Also, thanks goes out to Yasir Mohamed for an excellent organization of the workshop in Addis Ababa, Ethiopia. Thanks again to Bart, and Yasir, for giving me the chance to visit Africa, for the first time ever. My one week stay, although short compared to the almost one year work on this thesis, has given me quite an insight on the possible impact of climate (change) on the region.

Symbols and acronyms

IPCC	Intergovernmental Panel on Climate Change
AR4	Fourth Assessment Report
GCM	Global Circulation Model
SSTs	Sea Surface Temperatures
ENSO	El Nino/Southern Oscillation
CRU	Climate Research Unit
$^\circ$N	degrees North (latitude)
$^\circ$S	degrees South (latitude)
$^\circ$E	degrees East (longitude)
$^\circ$W	degrees West (longitude)
ITCZ	Intertropical Convergence Zone
mm	rainfall amount in millimeters, equivalent to liters per square meter
$^\circ$C	degrees Celsius
ZAB	Zaire Air Boundary
TEJ	Tropical Easterly Jet
hPa	hectoPascal
R	linear correlation
ΔP	Precipitation anomaly
GEV	Generalized Extreme Value
GHCN	Global Historic Climatology Network
RMS	Root Mean Square
ECMWF	European Centre for Medium-Range Weather Forecasts
ERA	ECMWF ReAnalysis
NCDC	National Climatic Data Center
ERSST.v2	Enhanced Reconstructed SST version 2
ESSENCE	Ensemble SimulationS of Extreme weather events under Nonlinear Climate changE
SRES	Special Report on Emissions Scenarios
P-E	Precipitation minus Evaporation
kg $m^{-1}s^{-1}$	kilograms per meter per second
LLJ	Low Level Jet
JAS	July, August and September
m/s	meters per second
tcw	total column of water
kg/m^2	kilograms per square meter
SH	Southern Hemisphere
CI	Confidence Interval

References

[1] Conway D. (2005): From headwater tributaries to international river: Observing and adapting to climate variability and change in the Nile basin. *Glob. Env. Change*, **15**, 99-114

[2] Endalew, G. J. (2007): Changes in the frequency and intensity of extremes over Northeast Africa. *KNMI*, **WR 2007-02**, pp46

[3] ESSENCE project page. <http://www.knmi.nl/ sterl/Essence/>

[4] Giannini et al. (2005): Dynamics of the boreal summer African monsoon in the NSIPP1 atmospheric model. *Clim. Dynam.*, **25**, 517-535

[5] Held, I. M. and Soden, B. J. (2006): Robust responses of the hydrological cycle to global warming. *J. Climate*, **19**, 5686-5699

[6] Hoerling et al. (2006): Detection and attribution of twentieth century Northern and Southern African rainfall change. *J. Climate*, **19**, 3989-4008

[7] Hulme M. and Tosdevin N. (1989): The Tropical Easterly Jet and Sudan rainfall: A review. *Theor. Appl. Climatol.* **39**, 179-187

[8] Hulme et al. (2001): African climate change: 1900-2100. *Clim. Res.*, **17**, 145-168

[9] IPCC (2007): Climate Change 2007: The Physical Science Basis. Contribution of Working Group I to the Fourth Assessment Report of the Intergovernmental Panel on Climate Change [Solomon, S., D. Qin, M. Manning, Z. Chen, M. Marquis, K.B. Averyt, M. Tignor and H.L. Miller (eds.)]. *Cambridge University Press*, Cambridge, United Kingdom and New York, NY, USA, 996 pp

[10] Lydolph, Paul E. (1985): The climate of the earth, Chapter 18 - Climate of Africa. *Rowman and Allonhelp, Publishers*

[11] Marsland, S.J., H. Haak, J.H. Jungclaus, M. Latif, and F. Roske (2003): The Max-Planck-Institute global ocean/sea ice model with orthogonal curvilinear coordinates. *Ocean Modelling*, **5**, 91-127

[12] Mitchell, T D. and Jones, P. D. (2005): An improved method of constructing a database of monthly climate observations and associated high-resolution grids. *Int. J. Climatology.*, **25 (6)**, 693-712, Royal Meteorological Society

[13] Nicholson, S. E. (2000): The nature of rainfall variability over Africa on time scales of decades to millenia. *Glob. and Plan. Change*, **26**, 147-158

[14] Oldenborgh, G.J. van et al. (2005): El Nino in a changing climate: a multi-model study. *Ocean Science*, **1**, 81-95

[15] Peterson, T. C., H. Daan, and P. D. Jones (1997): Initial selection of a gcos surface network. *Bull. Amer. Met. Soc.*, **78**, 2145-2152

[16] Roeckner, E., G. Bauml, L. Bonaventura, R. Brokopf, M. Esch, M. Giorgetta, S. Hagemann, I. Kirchner, L. Kornblueh, E. Manzini, A. Rhodin, U. Schlese, U. Schulzweida, and A. Tompkins (2003): The atmospheric general circulation model ECHAM 5. PART I: Model description, Report No. 349, *Max-Planck-Institut fur Meteorologie*, Hamburg, Germany, 127 pages

[17] Mxolisi Shongwe, Geert Jan van Oldenborgh, Bas de Boer, Bart van den Hurk (KNMI) and Maarten van Aalst (Red Cross/Red Crescent Climate Centre) (2006): Climate Change in Africa: Changes in extreme weather under global warming. <http://www.knmi.nl/africa_scenarios>

[18] Shongwe, Mxolisi. E., Geert Jan van Oldenborgh, Bart van den Hurk, Bas de Boer, Maarten van Aalst Caio A. S. Coelho (2007): Projected changes in extreme weather in Africa under global warming. *in preparation*

[19] Smith, T.M., and R.W. Reynolds (2004): Improved Extended Reconstruction of SST (1854-1997). *J. Climate*, **17**, 2466-2477

[20] Tippett and Giannini (2006): Potentially predictable components of African summer rainfall in an SST-forced GCM simulation. *J. Climate*, **19**, 3133-3144

[21] Uppala, S.M., Kållberg, P.W., Simmons, A.J., Andrae, U., da Costa Bechtold, V., Fiorino, M., Gibson, J.K., Haseler, J., Hernandez, A., Kelly, G.A., Li, X., Onogi, K., Saarinen, S., Sokka, N., Allan, R.P., Andersson, E., Arpe, K., Balmaseda, M.A., Beljaars, A.C.M., van de Berg, L., Bidlot, J., Bormann, N., Caires, S., Chevallier, F., Dethof, A., Dragosavac, M., Fisher, M., Fuentes, M., Hagemann, S., Hólm, E., Hoskins, B.J., Isaksen, L., Janssen, P.A.E.M., Jenne, R., McNally, A.P., Mahfouf, J.-F., Morcrette, J.-J., Rayner, N.A., Saunders, R.W., Simon, P., Sterl, A., Trenberth, K.E., Untch, A., Vasiljevic, D., Viterbo, P., and Woollen, J. (2005): The ERA-40 re-analysis. *Quart. J. Roy. Meteor. Soc.*, **131**, 2961-3012

[22] Williams, M. and Nottage, J. (2006): Impact of extreme rainfall in the central Sudan during 1999 as a partial analogue for reconstructing early Holocene prehistoric environments. *Quat. Int.*, **150**, 82-94

[23] Yeshanew A. and Jury M. R. (2007): North African climate variability Part 2: Tropical circulation systems. *Theor. Appl. Climatol.*, **89**, 37-49